Argonne National Laboratory

A STUDY OF THE DYNAMIC RESPONSE OF VARIOUS EBR-II CONFIGURATIONS TO HYPOTHETICAL MALFUNCTIONS IN THE REACTOR SYSTEM

by

A. V. Campise

Printed in the United States of America
Available from
Clearinghouse for Federal Scientific and Technical Information
National Bureau of Standards, U. S. Department of Commerce
Springfield, Virginia 22151
Price: Printed Copy $3.00; Microfiche $0.65

ANL-7613
Reactor Technology

ARGONNE NATIONAL LABORATORY
9700 South Cass Avenue
Argonne, Illinois 60439

A STUDY OF THE DYNAMIC RESPONSE OF VARIOUS EBR-II CONFIGURATIONS TO HYPOTHETICAL MALFUNCTIONS IN THE REACTOR SYSTEM

by

A. V. Campise

EBR-II Project

November 1969

TABLE OF CONTENTS

TABLE OF CONTENTS

LIST OF FIGURES

LIST OF FIGURES

LIST OF FIGURES

LIST OF FIGURES

LIST OF TABLES

LIST OF TABLES

NOMENCLATURE

A_j	Temperature coefficient of reactivity
C_p	Specific heat, Btu/lb-°F
H	Volumetric heat-generation rate, Btu/sec
i	Index for axial nodes in heat-transfer model
j	Index for radial nodes in heat-transfer model
k	Thermal conductivity, Btu/sec ft-°F
δK_c	Temperature-induced reactivity from change in sodium-coolant density, $
δK_f	Temperature-induced reactivity from fuel expansion, $
$\delta K_c^{A.R}$	Temperature-induced reactivity from change in sodium temperature in axial reflector, $
$\delta K_{c.r}^{R.R}$	Temperature-induced reactivity from growth in control-rod extension rod, $
N	Neutron density, n/cm^{-3}
NF	Number of feedback equations
P	Reactor power level (normalized to 1.0 at full power)
r	Reactivity, $
s	Laplace transform variable
t	Time, sec
t_i	Time to maximum reactivity insertion, sec
t_s	Time at which reactor trip signal is sensed, sec
$T_{B.F.}$	Blanket fuel (depleted-uranium) material temperature, °F
T_c	Coolant temperature, °F
T_F	Fuel temperature, °F
$T_c^{A.R.}$	Coolant temperature in axial reflector, °F
$T_c^{R.R.}$	Coolant temperature in radial reflector, °F
$T_{C.R.}$	Temperature of stainless steel control-rod extension rod, °F
T_D	Delay time, sec
UA	Overall heat-transfer coefficient
V	Volume, lb/ft^3
α_f	Temperature coefficient for fuel expansion, $/°F
α_c	Temperature coefficient for sodium density change, $/°F
γ_1	Linear input reactivity insertion rate, $/sec
γ_4	Maximum reactivity insertion, $
η	Viscosity, lb/ft-hr
θ	Inlet coolant temperature, °F
ρ	Density, lb/ft^3

A STUDY OF THE DYNAMIC RESPONSE OF VARIOUS EBR-II CONFIGURATIONS TO HYPOTHETICAL MALFUNCTIONS IN THE REACTOR SYSTEM

by

A. V. Campise

ABSTRACT

The dynamic response characteristics of various EBR-II irradiation-configuration loadings were investigated by using the space-independent kinetics code AIROS-IIA for dynamic simulation of the reactor system. The basic dynamic model was first used on system malfunctions outlined in the EBR-II Hazards Summary Report and shown to give very good agreement with published data. Subsequent irradiation core loadings were studied under various assumed hypothetical accident conditions to establish the details of the dynamic response of various metallic- and ceramic-fueled subassemblies. Dynamic response differences are noted under conditions of reduced and full coolant flow. Ceramic-fueled subassemblies will tend first to release activity under all transient conditions with full coolant flow. Conversely, metallic-fueled subassemblies will tend first to release activity under loss-of-flow conditions for all the cases studied.

I. INTRODUCTION

The Experimental Breeder Reactor II (EBR-II) is composed principally of a sodium-cooled reactor, an associated process system,[1,2] and a power plant with a design thermal-power capability of 62.5 MWt. The EBR-II core was designed to be fueled with either ^{235}U or plutonium. Currently it is fueled predominantly with ^{235}U. The EBR-II was originally designed as an engineering facility to determine the overall feasibility of this type of reactor for central-station, power-plant application.

In recent years the emphasis at EBR-II has been shifted toward its capabilities for irradiation in a fast-neutron flux. Using the EBR-II as an irradiation facility has involved testing various types of fast-reactor fuel elements that may change the dynamic characteristics of the core. Therefore, the continued safe and reliable operation of the EBR-II requires a constant surveillance of these dynamic characteristics. The required

safety surveillance involves a study of the EBR-II reactor and primary coolant system in terms of the neutronic and thermohydraulics characteristics of the reactor system and the interdependence of various inherent reactivity feedback networks. To simulate the EBR-II reactor dynamics accurately for several core loadings, the AIROS-IIA digital code[3] was programmed with various EBR-II core fuel-element characteristics. The AIROS-IIA code is a reactor-kinetics program with provisions for temperature-induced reactivity feedbacks. The AIROS-IIA code solves the space-independent reactor kinetics equation; it computes the temperature-induced reactivity feedback in the system by solving a set of equations representing the spatial heat- and mass-transfer model for several representative fuel channels in the EBR-II irradiation cores. The AIROS-IIA digital program was used to maintain a surveillance of the dynamic response characteristics of various irradiation cores.

In this study, four EBR-II cores are considered. The first core is the original EBR-II design core loading* listed in the Hazards Summary Report;[1] this core contained fuel elements of uranium-5 wt % fissium alloy. Three subsequent cores--each containing a varying complement of encapsulated experimental oxide-fuel elements--are also considered. These cores have been chosen to reflect core-component and reactor modifications that have had a primary influence on the dynamic response of the EBR-II. The component malfunctions considered here are similar to those listed in the Hazards Summary Report. These component malfunctions include abnormal operations of: (a) the control and safety rods, (b) the fuel-handling gripper mechanism, and (c) the primary coolant pumps. The various malfunctions are analyzed in the unprotected mode, i.e., no action by the protective system, and are followed to the onset of fuel melting in either a driver-fuel subassembly or an experimental subassembly.

Future studies of the dynamic response of the EBR-II irradiation facility will include detailed evaluations of the control and protective-system actions and of the various uncertainties in the physical properties of the materials introduced into the core for irradiation studies.

*Throughout this report "original loading" will refer to the EBR-II design core loading listed in the Hazards Summary Report.[1]

II. PHYSICAL CHARACTERISTICS OF VARIOUS EBR-II CONFIGURATIONS

A. Original EBR-II Design

The original EBR-II core had an equivalent diameter of 19.4 in., was 14.22 in. high, and had an active volume of 66.3 liters. It was fueled with elements of uranium-5 wt % fissium that had a fuel-pin diameter of 0.144 in., a sodium-bond annulus of 6 mils, and a cladding thickness of 9 mils. Figure 1 shows the general arrangement of reactor core and vessel,[4] and Fig. 2 presents a schematic of a standard driver-fuel subassembly containing 91 elements. Detailed design features of the original EBR-II core loading are given in Appendix D.

Table I lists the characteristics of the EBR-II as designed and as subsequently operated. Although the plant was designed to operate at 62.5 MWt, it was operated at 45 MWt until August 1968. The operating power was then raised to 50 MWt.* Moreover, the outlet sodium temperatures have been kept below 900°F, but the core volume has been increased from 66.3 to 91 liters. Finally, the complement of fueled experimental subassemblies has been varied between 10 and 20 as opposed to no experimental subassemblies in the original design study. In the kinetic analysis of the EBR-II core, two power levels will be considered: (a) 62.5-MWt design conditions, and (b) operation of EBR-II as an irradiation facility at 45 MWt.

Summarized in Table II are the results of the original thermal analysis of the maximum temperatures in the core and blanket of EBR-II at 62.5 MWt. Predicted and measured isothermal temperature coefficients for the original core are presented in Table III. These coefficients were used in constructing the feedback model for the original EBR-II core configuration at 62.5 MWt.

B. Various Irradiation Cores Containing Encapsulated Experimental Subassemblies

In support of the Liquid Metal Fast Breeder Reactor Program, EBR-II was operated at 45 MWt to irradiate a varying complement of encapsulated oxide, carbide, and metallic fuel elements. Table IV summarizes typical fuel-irradiation experiments in the core at various times during reactor operation, and Table V shows results of the thermal analysis of maximum temperatures of the metal driver fuel at 45 MWt.

The predominant experimental fuel elements have been plutonium and uranium oxides. Therefore, in studying the dynamic response of

*A demonstration run at 62.5 MWt was carried out during Sept 1969.

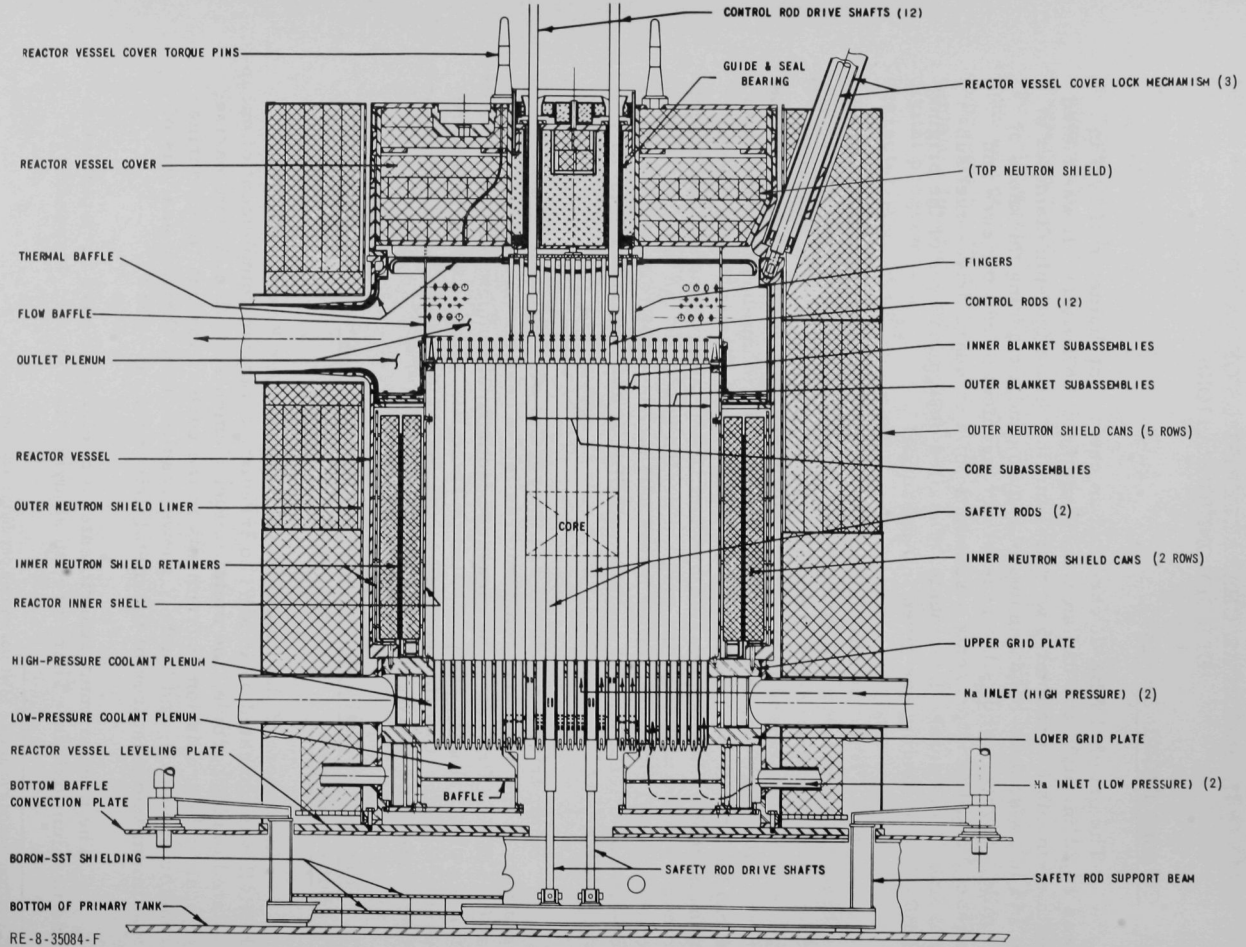

Fig. 1. EBR-II Reactor Vessel and Neutron Shield Assembly

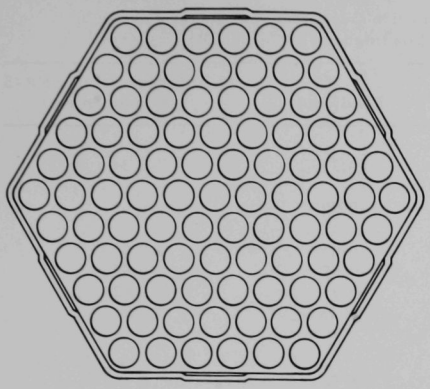

Fig. 2
Schematic of EBR-II Driver-fuel Subassembly

TABLE I. General EBR-II Physical Characteristics

System Parameter	EBR-II Design Conditions from Hazard Summary Report[1]	EBR-II Operating Conditions Analyzed Here
Reactor power, MWt	62.5	45[a]
Inlet sodium temperature, °F	700	700
Outlet sodium temperature, °F	900	832[b]
Reactor coolant flowrate, gpm	9200	9200
Core volume, liters	66.3	91
Number of experimental subassemblies	0	10-20

[a]Increased to 50 MWt in August 1968.
[b]Increased to 847°F in August 1968.

TABLE II. Maximum Temperatures in EBR-II Core and Blanket Elements at Reactor Power of 62.5 MWt

(No uncertainty factors)

	Core	Upper Blanket	Inner Blanket	Outer Blanket
Heat flux at element surface, Btu/hr-ft^2				
Maximum in zone	929,000	106,000	294,000	57,400
At point of maximum uranium temperature	571,000	84,800	279,000	< 300
Coolant flow in hottest subassembly				
Flow rate, Na at 800°F, gpm	93.7	93.7	31.0	5.0
Flow velocity, avg, fps	15.8	14.2	19.3	4.2
Temperatures in hottest channel, °F				
Uranium maximum	1,213	1,051	1,100	931
Coolant at outlet	1,037	998	906	931
Coolant at inlet	705	993	700	700
Coolant temperature rise, inlet to outlet	332	5	206	231
Coolant at point of maximum temperature	1,022	993	831	931
Temperature rises in hottest channel at point of maximum uranium temperature, °F				
Through uranium	105	33	186	0
Through uranium-sodium interface	7	1	4	0
Through sodium bond layer	8	2	10	0
Through sodium-clad interface	6	1	4	0
Through clad	39	15	52	0
Through coolant film	26	6	13	0
Total element temperature difference	191	58	269	0

Note: "Uranium" here means fuel alloy or blanket uranium, as appropriate.

TABLE III. Isothermal Temperature Coefficients of Reactivity in Original EBR-II Core Loading [in $(\Delta k/°C) \times 10^6$]

	Predicted	Inferred from ZPR-3 Measurements
Core		
Axial growth of fuel	-0.39	-0.34 ± 0.02
Radial growth of fuel (displacement of Na)	-0.09	-0.057
Axial growth of structure (density change)	-0.039	-0.033
Density change of coolant	-0.87	-0.98
Radial growth of support structure	-0.97	-0.92
Doppler effect	+0.04 (avg)	-
Bowing	-	-
Gaps		
Density change of coolant	-0.38	-0.33
Density change of structure	-0.036	-0.04
Upper and lower blanket		
Density change of coolant	-0.21	-0.21
Radial growth of uranium and jacket	-0.016	-
Axial growth of blanket uranium	-0.024	-
Axial growth of jacket	-0.021	-0.0064
Inner blanket		
Density change of coolant[a]	-0.2	-0.30
Axial growth of blanket uranium	-0.066	-
Axial growth of jacket[a]	-0.022	-0.054
Radial growth of uranium and jacket	-0.07	-
Radial growth of support structure	-0.17	-
Bowing	0	-
Outer blanket		
Density change of coolant[a]	-0.017	-0.011
Axial growth of blanket uranium	-0.014	-
Axial growth of jacket[a]	-0.003	-0.0012
Radial growth of support structure	-0.034	-

[a]The experimental results for these components are difficult to interpret because radial boundaries, especially between core and blanket, are not well defined.

TABLE IV. Summary of Typical Fueled Irradiation In-core Experiments

Experimental Subassembly No.	Type of Experiment	Power Generation, kW/ft	
		Maximum	Minimum
XO09	PuC-UC	28.0	19.6
XG05	UO_2-PuO_2	15.5	13.5
XA05	(Pu-U)C	26.0	17.2
XG06	UO_2-PuO_2	15.5	13.5
XA07	U-15 wt % Pu-9 wt % Zr	9.4	8.2
XO11	UO_2-20 wt % PuO_2	23.0	19.5
XO12	UO_2-20 wt % PuO_2	15.5	13.5
XO15	UO_2-20 wt % PuO_2	15.4	14.0
XO17	UO_2-20 wt % PuO_2	15.4	13.5
XO19	UO_2-20 wt % PuO_2	8.0	7.0
XO20	UO_2-PuO_2	8.0	7.0

TABLE V. Maximum Temperatures in EBR-II Core and Blanket Elements at 45.0-MWt Reactor Power

(No uncertainty factors)

	Core	Upper Blanket	Inner Blanket	Outer Blanket
Heat flux at element surface, Btu/hr-ft^2				
Maximum in zone	669,000	75,400	212,000	41,300
At point of maximum uranium temperature	377,000	61,000	192,000	< 200
Coolant flow in hottest subassembly				
Flowrate of Na at 800°F, gpm	68.2	68.2	22.6	4.3
Flow velocity, avg, fps	11.5	10.3	13.9	3.0
Temperatures in hottest channel, °F				
Uranium, maximum	1,106	1,032	1,024	929
Coolant, at outlet	1,033	995	904	929
Coolant, at inlet	705	990	700	700
Coolant temperature rise, inlet to outlet	328	5	204	229
Coolant, at point of maximum uranium temperature	1,033	990	838	929
Temperature rises in hottest channel at point of maximum uranium temperature, °F				
Through uranium	69	24	128	0
Through uranium-sodium interface	5	1	3	0
Through sodium bond layer	5	1	7	0
Through sodium-clad interface	4	1	3	0
Through clad	26	11	35	0
Through coolant film	18	4	10	0
Total element temperature difference	127	42	186	0

Note: "Uranium" here means fuel alloy or blanket uranium, as appropriate.

irradiation cores containing encapsulated fuel elements, a typical mixed-oxide fuel element was chosen as being indicative of the response of most irradiation experiments. The oxide-fuel elements were contained in the EBR-II experimental irradiation subassembly shown in Fig. 3. The basic fuel element was enclosed in a stainless steel capsule with sodium bonding for heat transfer to the flowing coolant outside the capsule. Table VI summarizes the typical characteristics of the EBR-II experimental fuel element.

Several irradiation core loadings studied are listed in Table VII. These core loadings correspond to various reactor "runs" of several hundred megawatt-days each. Runs 16, 24, and 26 are considered typical of the irradiation cores into which major core modifications have been introduced, and which thereby affect the dynamic characteristics of the reactor. Figures 4 through 7 illustrate the grid loadings for these various cores and show the positions of the experimental subassemblies by X-series designations.

The temperature coefficients for the various core configurations were obtained by using S_2 calculations with an R-Z representation of the EBR-II core.[5] The cross-section set used for these calculations has agreed with the EBR-II studies of ZPR-3 critical configuration as well as with the EBR-II wet-critical configuration; these cross sections are considered representative of the environment in the EBR-II core. The temperature coefficients are presented in Table VIII; the temperature-induced feedback values based on these coefficients were used in constructing a dynamic model to describe the response of various EBR-II irradiation cores.

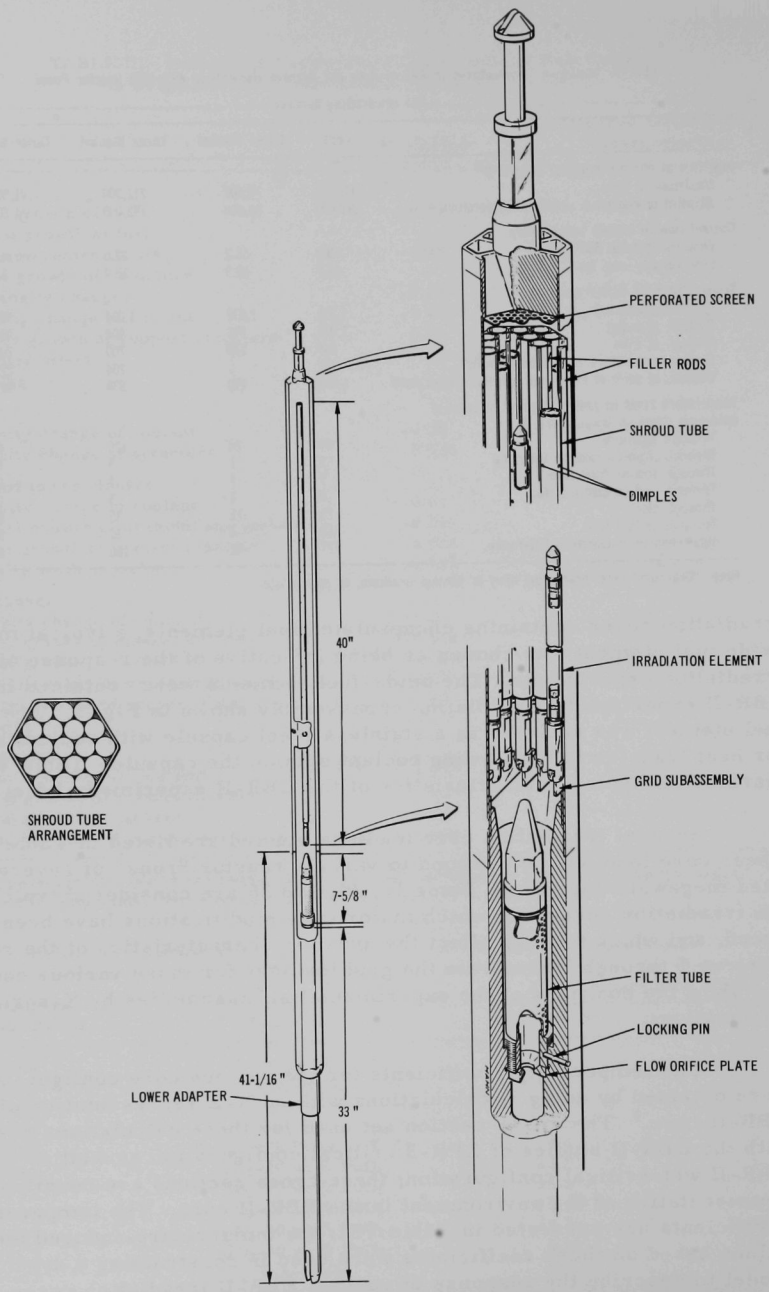

Fig. 3. EBR-II Experimental Irradiation Subassembly (Mark A)

TABLE VI. Physical Characteristics of EBR-II Irradiation Core Fuel Elements

Fuel-element Parameter	Metallic Driver Fuel		Typical Oxide Experiment
	Mark I	Mark IA	
Cladding OD, in.	0.174	0.174	0.082
Cladding ID, in.	0.156	0.156	0.252
Cladding thickness, in.	0.009	0.009	0.015
Na-annulus thickness, in.	0.006	0.006	Helium-bonded 3-mil gap
Fuel-pin diameter, in.	0.144	0.144	0.250
Fuel-element length, in.	14.2	13.5	14.2
Effective fuel density, %	85	85	90

TABLE VII. Physical Properties of EBR-II Irradiation Cores

Item	Run 16 (end)	Run 24 (end)	Run 25 (end)	Run 26 (start)
Number of subassemblies in core	75	81	88	91
Material of inner radial blanket[a]	Depleted U	Depleted U	Steel	Steel
Fuel type	Mark I	Mark IA	Mark IA	Mark IA
Axial-blanket material	Depleted U	Steel	Steel	Steel
Axial-blanket design	Pin	Pin	50 Pin; 13 Trifluteb	33 Pin; 31 Triflute[b]
Number of experiments	5	9	11	13
Average core sodium temperature, °F	791	787	792	792
Average fuel temperature, °F	911	911	911	911
Average core steel temperature, °F	830	825	828	828
Expansion of core radius, cm[c]	0.0347	0.0349	0.0364	0.0370
Average sodium temperature in upper axial blanket, °F	881	876	884	884

[a]Rows 7 and 8 of the EBR-II grid.
[b]Number of subassemblies with each design.
[c]Expansion of reactor grid plate support.

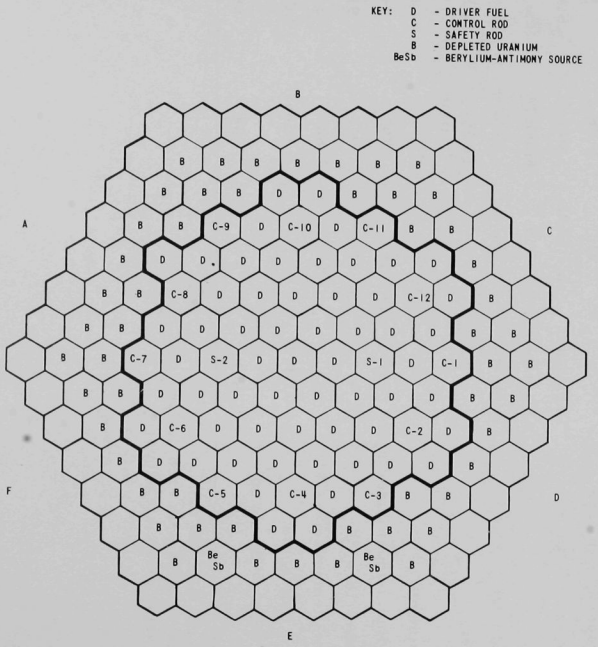

Fig. 4. EBR-II Loading Pattern: Run 1

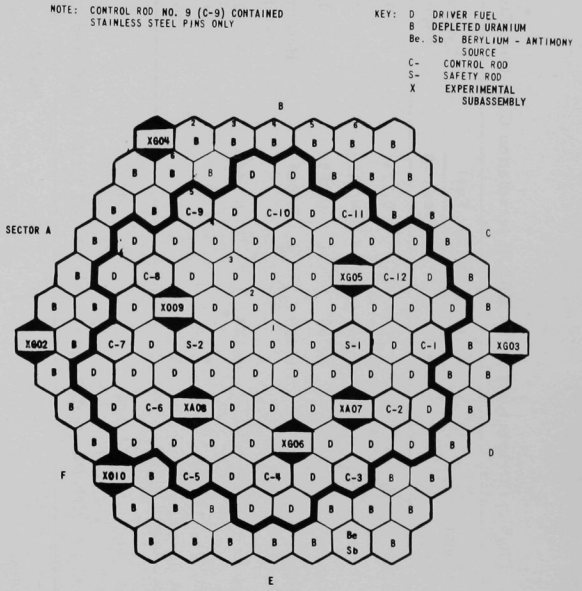

Fig. 5. EBR-II Loading Pattern: Run 16

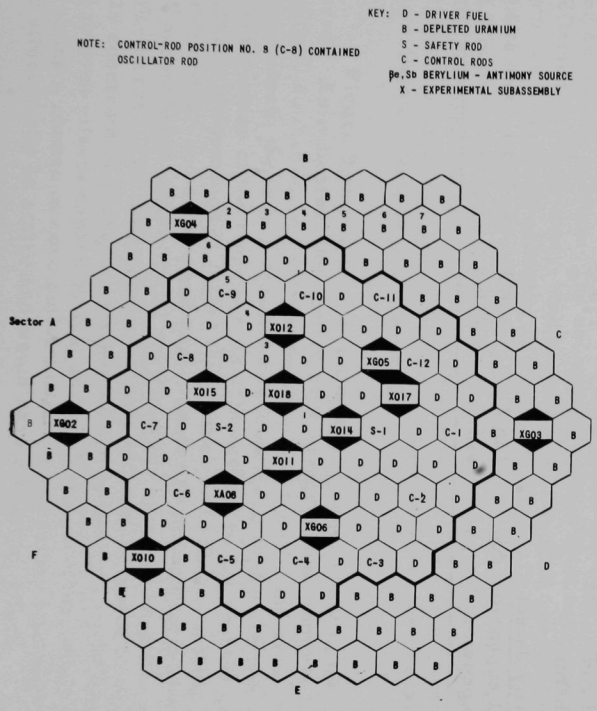

Fig. 6. EBR-II Loading Pattern: Run 24

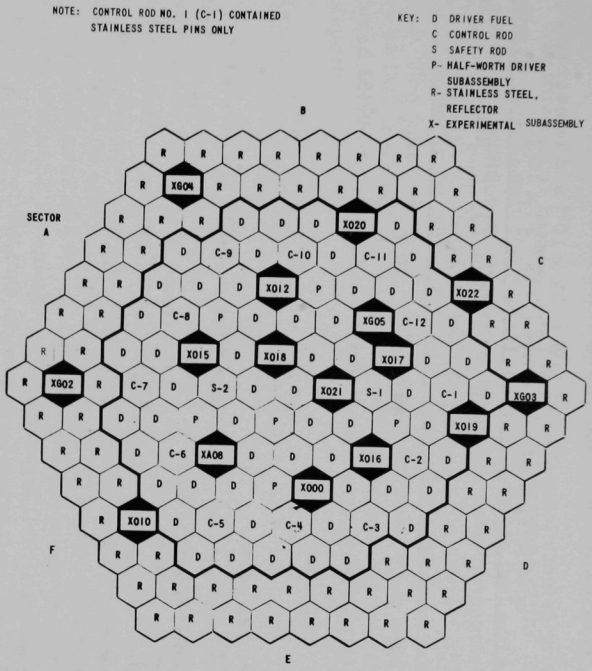

Fig. 7. EBR-II Loading Pattern: Run 26

TABLE VIII. Calculated Values of Components of EBR-II Power Coefficient

Reactivity defects from 0 to 45 MW [$-\Delta k \times 10^5$] and temperature coefficients of reactivity [$(-\Delta k/°F) \times 10^5$]

Item	Run 16 (end)	Run 24 (end)	Run 25 (end)	Run 26 (start)
Sodium in core, Δk	44.7	40.7	43.6	40.8
Sodium in core, $\Delta k/°F$	0.494	0.465	0.481	0.462
Sodium, upper reflector blanket, Δk	29.6	30.9	40.7	40.1
Sodium, upper reflector blanket, $\Delta k/°F$	0.160	0.189	0.223	0.222
Sodium, in radial blanket, Δk	5.9	7.2	3.6	3.2
Sodium, total, Δk	80.4	79.0	88.2	84.5
Fuel, Δk	44.6	43.6	42.3	4.15
Fuel, $\Delta k/°F$	0.211	0.206	0.200	0.196
Steel expansion				
Axial, Δk	8.7	9.1	12.4	17.9
Axial and radial, Δk	119.6	118.2	122.0	129.3
Radial, Ih/mil	3.8	3.4	3.3	3.3
Total reactivity defect				
No radial expansion, Δk	135.2	138.1	152.1	147.7
Radial expansion, Δk	225.3	250.3	255.7	253.9

III. MODEL FOR DYNAMIC SIMULATION OF THE REACTOR

In this initial review of the dynamic response of the EBR-II irradiation cores, only the prompt feedbacks due to fuel and sodium coolant were considered. However, there are other important feedback networks in the EBR-II core, and these will be the subject of a detailed feedback model in future analytical studies of the dynamic response of EBR-II. The following three sections review these other feedback networks so that their effect on the outcome of the various transients can be evaluated with reference to the subsequent kinetic analysis presented in this report.

A. Reactor Tank and Vessel Arrangement

Figure 8 is a schematic of the primary reactor tank and vessel showing the primary-coolant flow path.[4] Included are the high- and low-pressure plena, the grid structure supporting the reactor core, and the blanket region. Although a small, negative structural feedback from the expansion of the core-support structure during the rise to power exists, this contribution is not included in the feedback model used in this study. Figure 8 also shows the primary-coolant-pump suction and flow through the primary magnetic flowmeters where coolant flow is normally indicated. However, in a study of the loss of primary coolant flow, these flowmeter indications are assumed to be inactive. Also shown in Fig. 8 is the inlet for secondary sodium. The secondary-sodium inlet temperature is reflected in the primary-tank coolant by a long time constant (several minutes as opposed to tenths of a second). This difference in time constants has been observed in various systems studies. However, the effect of this difference has been omitted by assuming that the primary-coolant inlet temperature to the reactor is constant at 700°F. In future reports all these system variations will be included to study the overall effects on the dynamic response of the EBR-II core.

Figure 9 shows details of the major components in the reactor vessel. As indicated, the control rods are grappled from the top of the reactor, so that during operations involving a change in core outlet-sodium temperature, there is a reactivity feedback due to the relative expansion or contraction of the control rods with respect to the reactor core. This feedback phenomenon is called the control-rod effect. Heating of the core outlet sodium and subsequent heat transfer to the control-rod supports are not included in this initial review of the dynamic response of the EBR-II core. The time constant of this effect is believed to vary over a wide spectrum of characteristic times and is not as well-known as are the prompt effects caused by fuel and coolant. However, in all transients involving a change in core outlet-sodium temperature this negative control-rod effect would be active and would have a limiting effect.

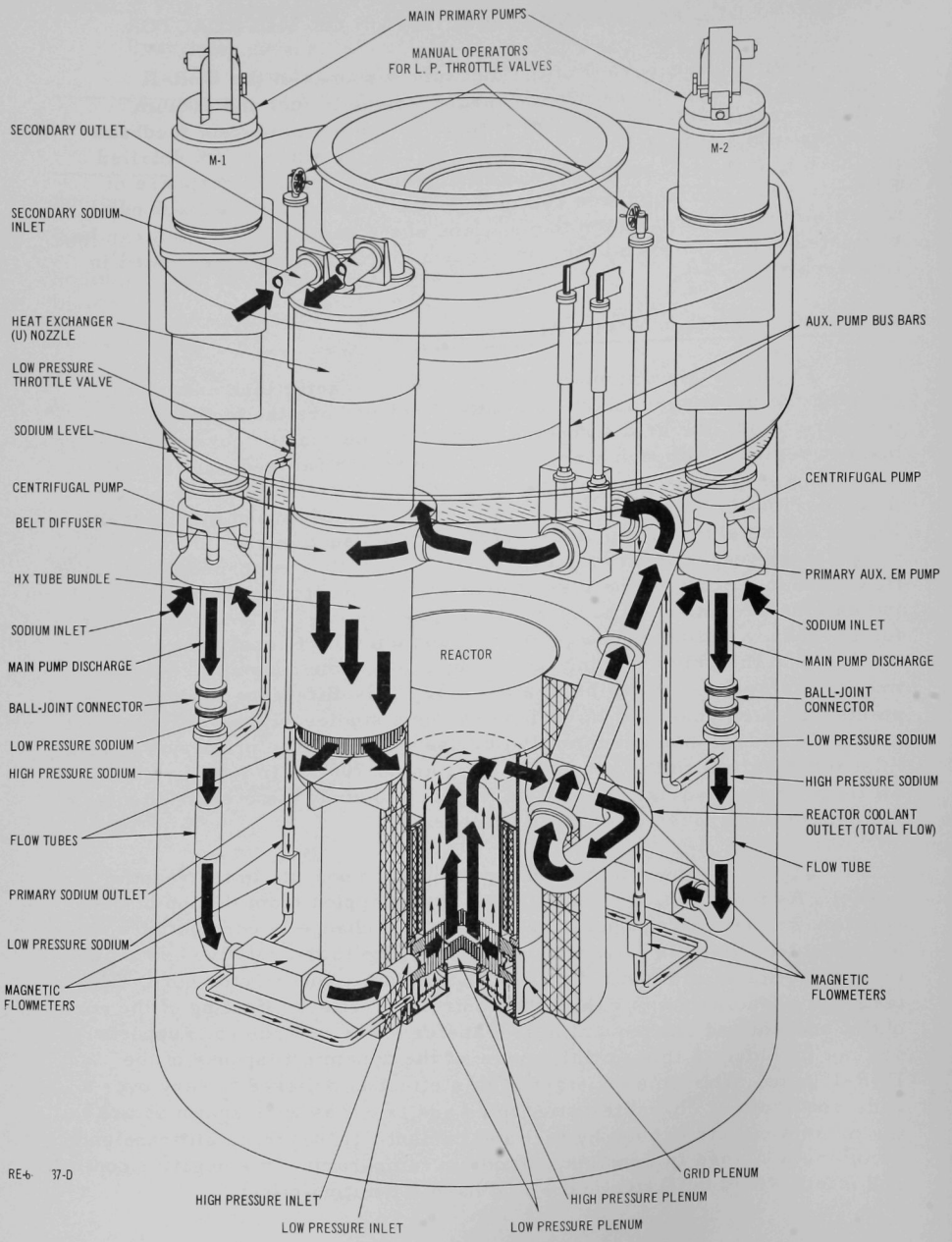

Fig. 8. Primary Cooling System

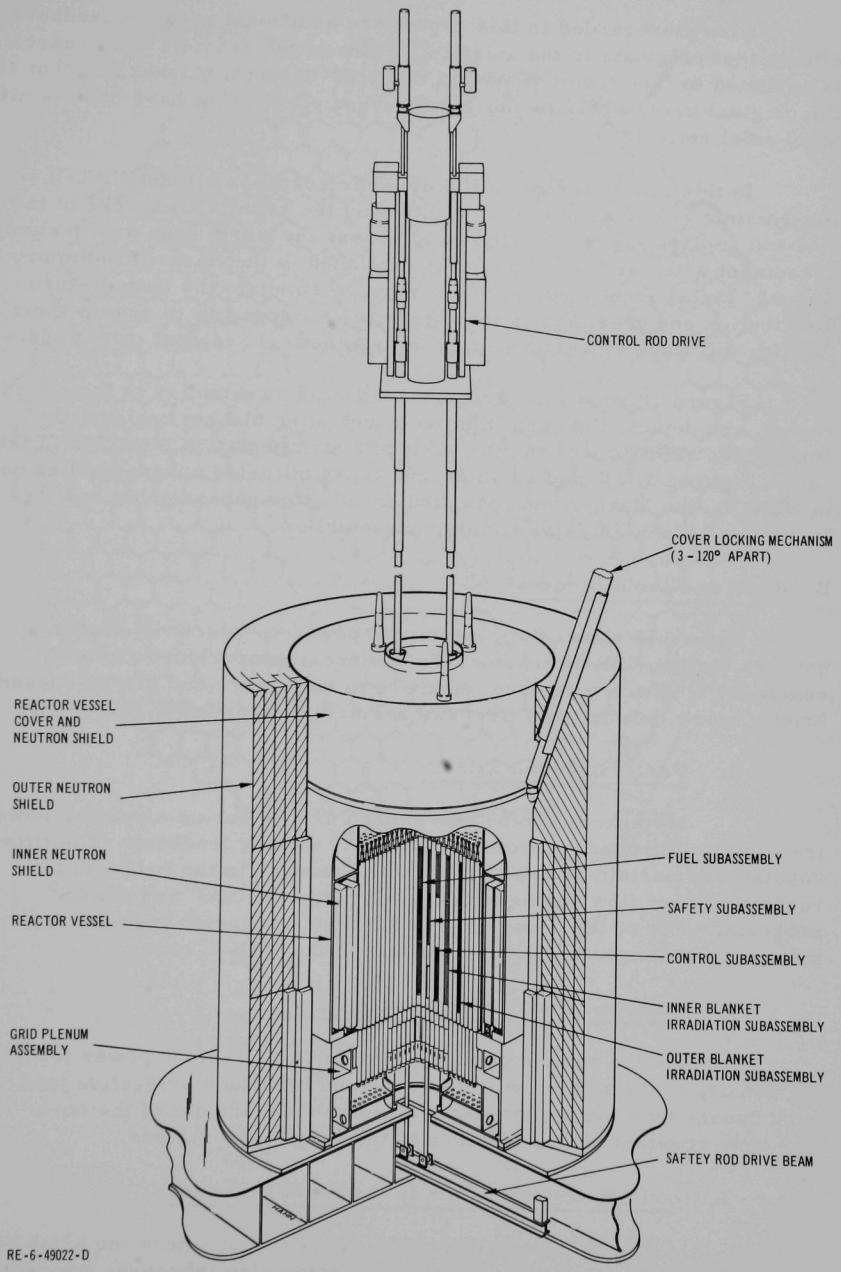

Fig. 9 Cutaway of EBR-II Showing Location of Major Components

Also disregarded in this report are additional negative feedback effects that originate in the axial reflectors of the reactor. The reactor is assumed in this report to have a depleted-uranium blanket like that of the original core, whereas subsequent irradiation cores have had stainless steel axial reflectors.

In this initial review of the dynamic response of past EBR-II cores, the dynamic response of the core with only the prompt feedbacks of the fuel and coolant has been analyzed to assess the worst case and to show agreement with earlier calculations published in the Hazards Summary Report.[1] Subsequent studies will attempt to simulate the temperature distribution and gradients in the other core components to assess their limiting influence on various types of hypothetical accident conditions.

Figure 10 shows the arrangement of subassemblies in the reactor vessel, and depicts the core, the inner and outer blanket regions, the control and safety rods, and the various instrumentation locations in the core. Figures 3, 11, and 12 show four types of fueled subassemblies used in EBR-II: the Mark-A encapsulated-irradiation subassembly and the Mark-I and Mark-IA driver-fuel subassemblies.

B. Reactor Feedback Model

Figure 13 shows the generalized power-to-reactivity feedback network for the EBR-II reactor. Six different temperature-induced reactivity feedback paths are identified in this figure and are discussed briefly below, but only the first two are actually applied in this study.

1. Fuel-expansion Effect

Metallic fuel pins will expand axially during a reactor power transient to introduce a prompt negative reactivity feedback. The time constant for certain prompt temperature changes in the fuel with full reactor coolant flow has been computed by the ARGUS[6] and AIROS[3] programs to be of the order of 0.3 sec. Fuel expansion in metal fuel pins is the most prompt feedback effect in the EBR-II core.

2. Sodium-density Effect in the Core

As the sodium coolant heats during a reactor power transient, the density of the sodium will decrease and introduce a negative feedback caused by a strong increase in neutron leakage out of the core. The time constant of this effect is in the range 0.15-0.2 sec.

3. Sodium-density Effect in the Axial Reflector

As the sodium is heated in the core and enters the axial reflector, the decreased density in that region also increases the neutron

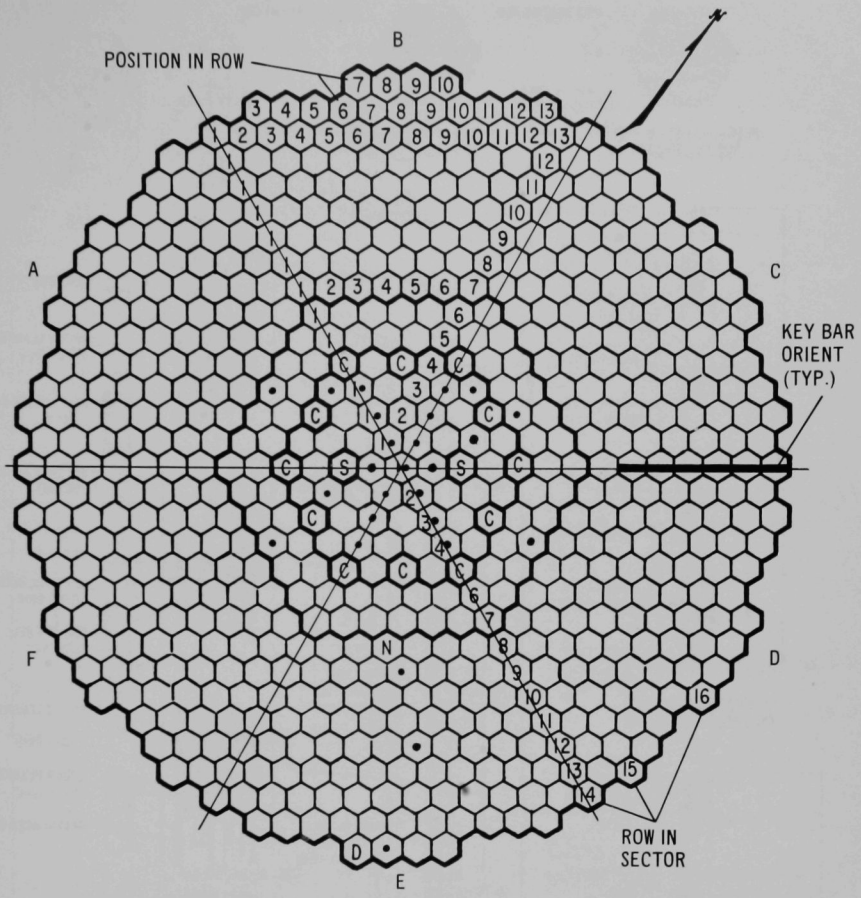

LEGEND

1.	SECTORS	A to F
2.	CONTROL RODS (12)	C
3.	SAFETY RODS (2)	S
4.	THERMOCOUPLES (26)	•
5.	FIXED DUMMY	D
6.	NEUTRON SOURCE	N
7.	GRID POSITIONS	
	CORE	61
	INNER BLANKET	66
	OUTER BLANKET	510
	TOTAL	637

RE-6-49021-B

Fig. 10. Subassembly Arrangement in the Reactor Vessel

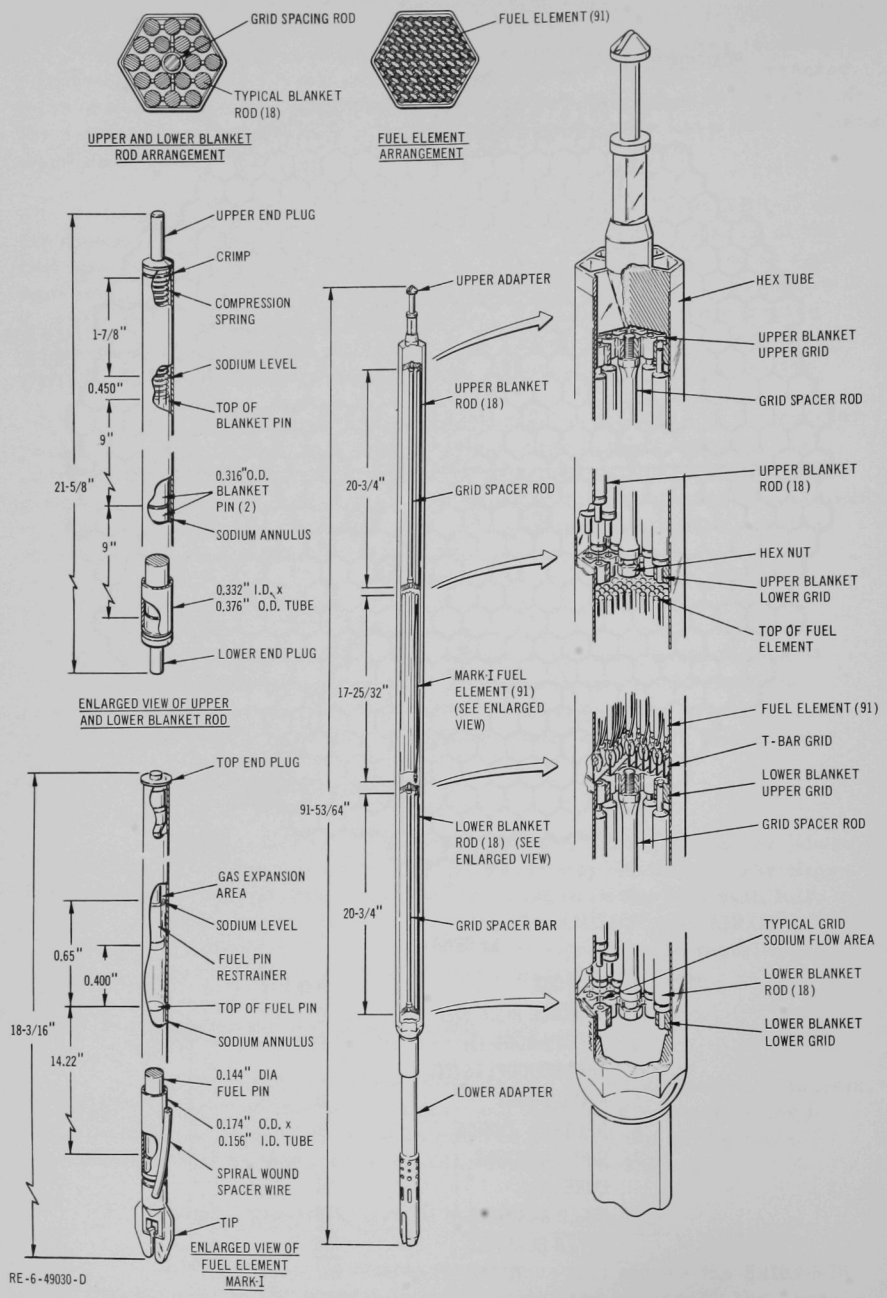

Fig. 11. EBR-II Mark-I Driver-fuel Subassembly (with Uranium Blankets)

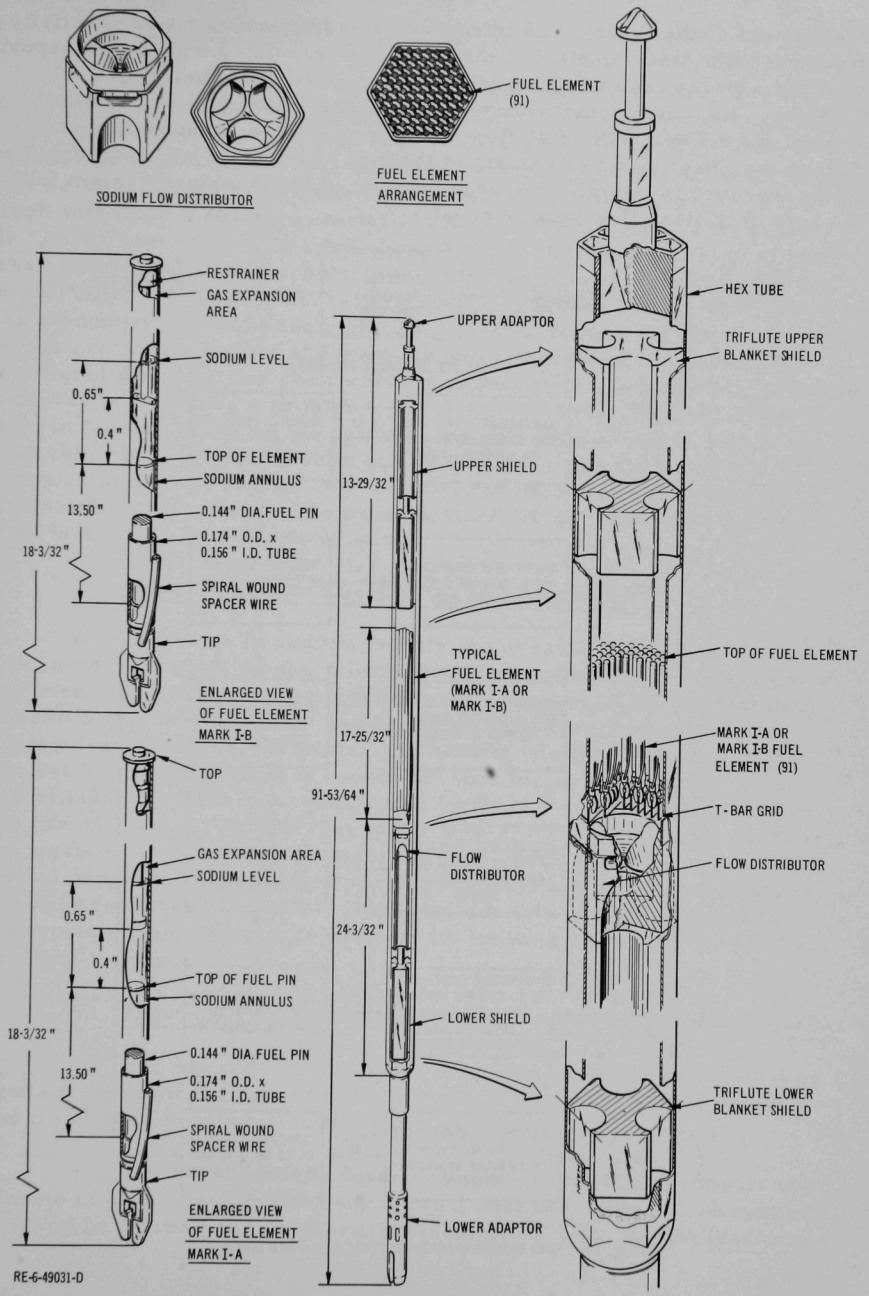

Fig. 12. EBR-II Mark-IA and Mark-IB Driver-fuel Subassemblies (with Axial Stainless Steel Reflectors)

leakage out of the reactor and introduces an additional negative reactivity feedback. The time constant of this effect is associated with the transport time through the core and the sodium density, and is in the range 0.20-0.25 sec. The combined effective time constant of the fuel and sodium coolant is ~0.5 sec under full-flow conditions. Under reduced-flow conditions the effective time constant of the fuel and coolant will increase due to the increase in the effective heat capacity of the combined system in the absence of coolant-flow heat removal.

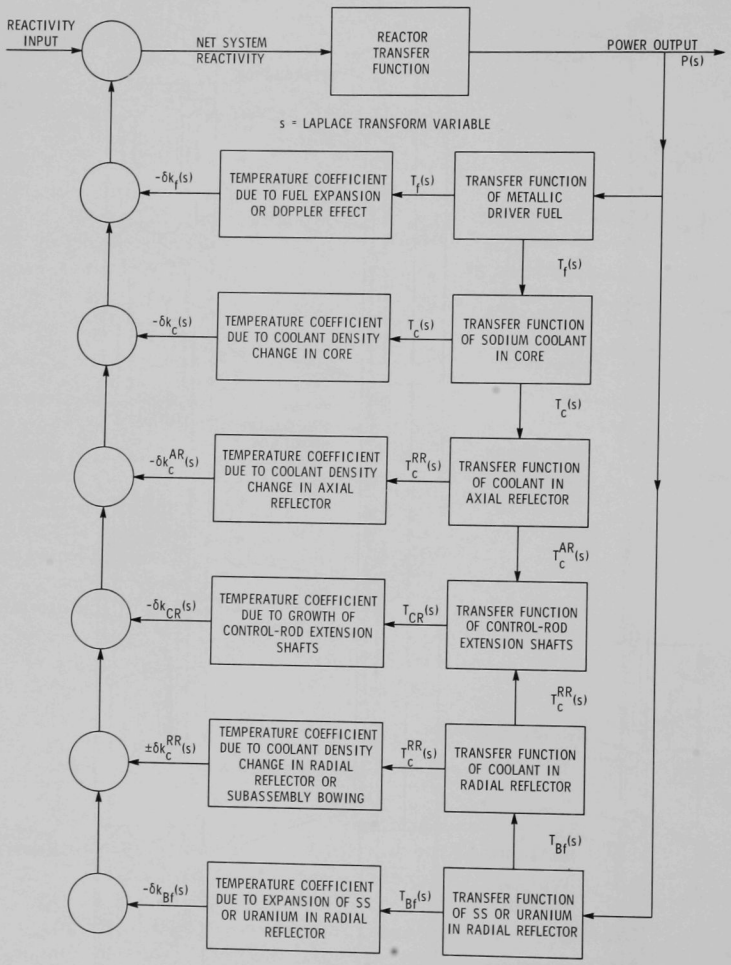

Fig. 13. EBR-II Power-to-Reactivity Feedback Network

4. Control-rod Effect[7]

The control-rod extension shafts extend from the primary-tank cover (through the reactor-vessel cover) into the active core. An extension shaft has a varied and complex temperature gradient across it during steady-state conditions. For example, during a transient the shaft heating and relative control-rod motion caused by temperature changes in the shaft introduce a negative reactivity effect in the reactor. This effect is further complicated by nonuniform heating of certain portions of the shaft by various sodium-coolant streams. The portion inserted into the active core is heated by core-outlet sodium, whereas the portion located in the plenum is heated by the bulk outlet reactor sodium that includes cooler sodium from the blanket and from the outer regions of the core. That portion of the extension shaft which is heated by the core-outlet sodium is believed to introduce a prompt negative effect. This effect will be evaluated in future studies on the dynamic response of the EBR-II core. Subsequent heating by bulk sodium and by changes in the bulk-sodium temperature in the reactor tank are delayed but may be important in loss-of-flow transients. The time constant[6] for the control-rod effect may thus range from 0.1 to 20 sec.

5. Sodium-density Effect in the Radial Blanket

A change in sodium density in the radial blanket will produce a negative reactivity feedback because of increased radial leakage out of the core. This effect is prompt, but small, because of the low worth of sodium in the radial blanket and the small temperature change in the depleted-uranium fuel elements. Included in this feedback path is the blanket bowing effect that is associated with the sodium coolant in the radial blanket. This is a complicated feedback,[6] and it has varied over the life of EBR-II. At different power levels, the effect may be positive or negative, and an additional subroutine is required in the basic AIROS digital program to handle this varying effect. Further studies of the dynamic response of the EBR-II will include this phenomenon and the appropriate time constant to evaluate its limiting effect on the various accident sequences.

6. Expansion of Stainless Steel or Uranium in the Radial Blanket

The negative feedback due to expansion of stainless steel or uranium is small because of the low worth of the materials in the blanket and the small temperature differences experienced.

The six feedbacks described above constitute the major components of a generalized feedback network that describes the phenomena involved in limiting any reactor transients in EBR-II. All feedbacks are

negative with the one exception of blanket-subassembly bowing, which may be positive or negative. In this first review of the dynamic response of various EBR-II cores, only the first two prompt feedback paths have been followed. Subsequent transient studies will introduce the last four feedback networks for a comprehensive evaluation of the dynamic characteristics of various EBR-II irradiation cores.

Table IX shows the basic delayed-neutron data and other kinetic data used to simulate the reactor kinetics of EBR-II. (The contribution from plutonium-fueled experiments is negligible.)

TABLE IX. EBR-II Reactor-kinetics Data

Delayed-neutron Group	A_i[a]	λ_i[b]	Delayed-neutron Group	A_i[a]	λ_i[b]
1	0.0347	0.0127	4	0.4041	0.3110
2	0.2034	0.0317	5	0.1406	1.400
3	0.1847	0.1150	6	0.0325	3.7800

$\beta_{eff} = 7.44 \times 10^{-3}$; $\ell_p = 1.55 \times 10^{-7}$ sec.

[a]Relative abundance.

[b]Decay constants.

C. Fuel-element Channels

The thermal-kinetics studies of various EBR-II driver-fuel and irradiation-test elements were based on cylindrical geometry with three axial nodes in each region of the fuel element. Three axial nodes were used in the metallic driver fuel for EBR-II: sodium bond, cladding, and coolant channel. In the oxide element, there were also three axial nodes in the fuel: helium gas gap, cladding, and coolant channel. These fuel-channel models are shown in Figs. 14 and 15.

Only two types of fuel channels were utilized in the dynamic simulation of the original EBR-II core. The first channel was called the peak fuel-element channel, in which peak temperatures in each heat-transfer node were computed. The second channel was called the feedback fuel channel, in which the temperature changes were characteristic of the major portion of the core. These characteristic temperature changes were associated with a temperature coefficient of reactivity to compute the power-to-reactivity feedback in a given power transient.

In the study of the various irradiation cores with experimental oxide elements, a five-channel representation was used. This representation was applied to the following types of elements:

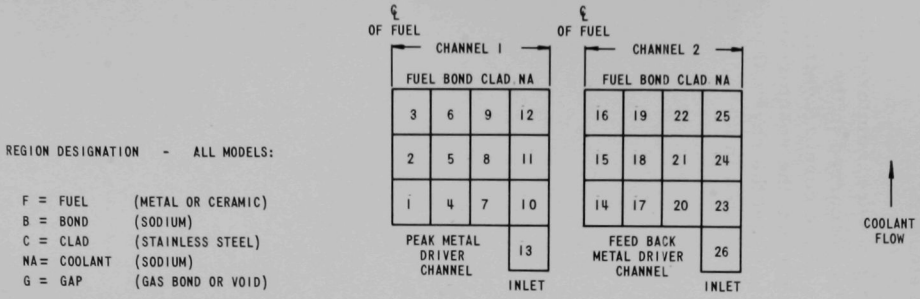

Fig. 14. EBR-II Two-channel Model, Showing Numbering of Nodes for Thermal-kinetics Studies

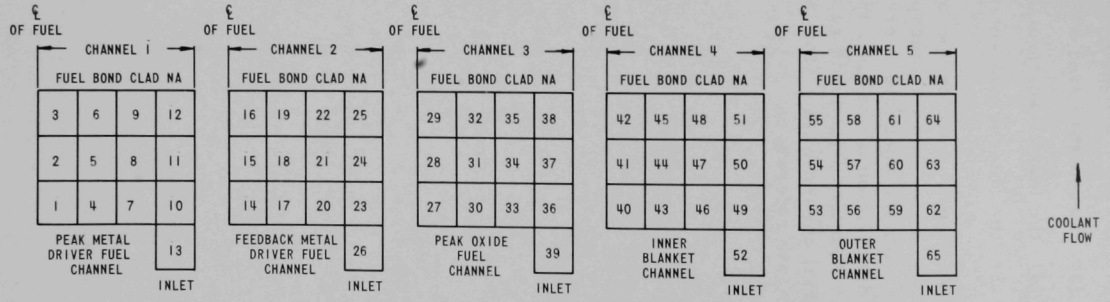

Fig. 15. EBR-II Five-channel Model, Showing Numbering of Nodes for Thermal-kinetics Studies

(1) the peak metallic driver-fuel element,

(2) the feedback metallic driver-fuel element,

(3) the encapsulated oxide-fuel element,

(4) the inner-radial-blanket fuel element, and

(5) the outer-radial-blanket fuel element.

Various reactor temperature changes were monitored during these studies to ensure that no unexpected effect occurred in the transient and that there was an adequate representation of the core. A detailed theoretical description of the heat-transfer equation, the reactor-kinetics equation, the reactivity-feedback representation, and the physical properties of the material chosen in this simulation are presented in the Appendixes with appropriate references.

IV. KINETIC RESPONSE OF VARIOUS IRRADIATION CORES

The kinetic response of various irradiation cores was examined in the unprotected mode (i.e., no action by the protective system to limit the transient by sensing changes in the reactor environment). All transients except the loss-of-coolant-flow accident were carried to the onset of fuel melting in the peak EBR-II fuel element or in the experimental oxide specimens. These initial investigations were not carried past the threshold of fuel melting because of the complicated phenomena that would occur. Future studies will cover the initial phases of fuel melting and coolant boiling as well as the potential interaction between driver fuel and its cladding, and will evaluate their influences on more severe core conditions in the EBR-II. In addition, the changes in the physical properties and configurations of irradiated fuel elements will be studied for their influence on the transient behavior of EBR-II cores.

A. Component Malfunctions Considered

Six hypothetical reactivity accidents and several loss-of-coolant-flow sequences were considered in the EBR-II Hazards Summary Report.[1] These accidents were chosen to describe the threshold of fuel melting and thereby the initiation of more severe temperature conditions. Each malfunction sequence requires the complete inoperability of the control and protective system as well as the loss of administrative control. Many protective-system interlocks must be bypassed and existing circuits made inoperative for these accident conditions to prevail until the onset of core damage. Therefore, in the following study of the dynamic response of the EBR-II core, we have picked the inherent safety characteristics of the core in these hypothetical nuclear incidents, and thus have to assume an inconceivable breakdown in the control and protective system and an incredible lack of administrative control to carry out the analysis. All reactivity-induced cases assume either full coolant flow through primary circuit or reduced flow (≈5.5% of full flow). A flowrate of ~5.5% was chosen to simulate induced thermal convection in the core when the primary pumps are turned off during shutdown and fuel handling. Only Case 7 of the seven considered below assumes loss-of-coolant flow.

Case 1--The reactor is at the delayed-critical condition (zero power) with the safety rods out of the core. (The safety rods in EBR-II are fuel subassemblies.) The safety rods are assumed to be driven into the active core in an uncontrolled manner at their normal speed of approximately 2 in./min.

Case 2--The reactor is at the delayed-critical, zero-power condition with the central driver-fuel subassembly removed. The central subassembly is then assumed to be loaded into the core at a regular speed of 6 in./min.

Case 3--The reactor is at the delayed-critical, zero-power condition with a single control rod removed. The control rod is then assumed to be driven into the core in an uncontrolled sequence at 5 in./min.

Case 4--This case is similar to Case 3 except that the power transient begins at full operating power (62.5 MWt for the original core and 45 MWt for the experimental cores).

Case 5--In this hypothetical accident the reactor is assumed to be at the delayed-critical, zero-power condition with a central driver-fuel subassembly being loaded into the core. A failure is then assumed to occur in the grapple mechanism, thereby dropping a driver-fuel subassembly into the core. In this condition, reactivity adds rapidly. This is the classic hypothetical startup accident; its occurrence in EBR-II would require many simultaneous malfunctions or maloperations or both.

Case 6--The reactor is at delayed-critical, zero-power condition with a central driver-fuel subassembly removed. This subassembly is then introduced at the highest speed of the gripper mechanism (72 in./min) to cause a rapid rise in reactivity in the reactor.

Case 7--This hypothetical accident is the only sequence involving loss of coolant flow. The accident sequence is initiated by a reactor trip, followed by the loss of primary pumping power. The subsequent temperature transient is evaluated.

All seven hypothetical accident sequences were applied to the original EBR-II core loading. Subsequent core loadings containing oxide fuel were subjected only to Cases 1, 2, and 4, which are sufficiently indicative of the dynamic responses of these cores. These three cases include an at-power accident and two just-critical startups with a range of reactivity insertions.

No credibility is given to actual occurrence of these accident sequences. However, these hypothetical accidents test the inherent safety characteristics of the EBR-II irradiation cores, and they provide some basis for comparison of various core dynamic responses and their qualitative effect on plant safety.

B. Original EBR-II Design at 62.5 MWt

The AIROS-IIA digital program was used to simulate the seven hypothetical malfunction cases described above. Table X shows the assumed reactivity ramp rates for six of the seven accident sequences. This table also shows the reactivity ramp rates inferred from measured values for various core components in the ZPR-3 critical assembly. Some results obtained by using these measured values on various accident cases are presented in the appendixes.

TABLE X. Assumed Reactivity Ramp Rates Used for Malfunction Studies of Original EBR-II Core

Accident Simulation	Reactivity Ramp Rates in EBR-II, $/sec	
	Hazard Summary Report	Inferred from ZPR-3 Measurements[a]
1. Safety rods driven into just-critical core	0.00667	0.0033
2. Central driver-fuel subassembly driven into just-critical core	0.0200	0.0146
3. One control rod driven into just-critical core	0.0040	0.0028
4. One control rod driven into core at 62.5 MWt	0.0040	0.0028
5. Central driver-fuel subassembly dropped into just-critical core	13.2	5.6
6. Central driver-fuel subassembly driven at high speed into just-critical core	0.24	-

[a]Inferred from ZPR-3 critical-assembly measurements.

1. Full Coolant Flow

Under full coolant flow all seven hypothetical accident cases are considered.

a. Case 1--Figure 16 shows the power increase during the original loading at full coolant flow following an inadvertent insertion of the EBR-II safety rods into a just-critical core. Figure 17 shows the subsequent temperature increase in the peak metallic driver-fuel element. The first temperature response occurs 80 sec after the beginning of the insertion of the safety rods (indicating the effect of starting the transient at very low power). The maximum heating rate obtained during this transient is 37°F/sec. At this time the reactor period attains its minimum of 2.9 sec. The onset of centerline fuel melting in the peak driver element occurs 121 sec after the accident sequence starts. At the time of melting, the reactor period has lengthened to approximately 44 sec, indicating the effect of the prompt feedback from the fuel and coolant. The maximum reactivity inserted during this transient sequence is approximately 60¢, with the net system reactivity reduced to 23¢ due to the temperature rise of the metallic driver fuel. Figure 17 shows the peak cladding temperature at fuel melting to be approximately 1390°F, whereas the coolant temperature is only 1260°F. When the peak metallic driver fuel reaches centerline melting, the fuel in the feedback channel will have attained a temperature of 1690°F, which is still below the melting point of the fuel.

b. Case 2--The central driver-fuel subassembly is inserted into a just-critical core configuration during the original loading at full

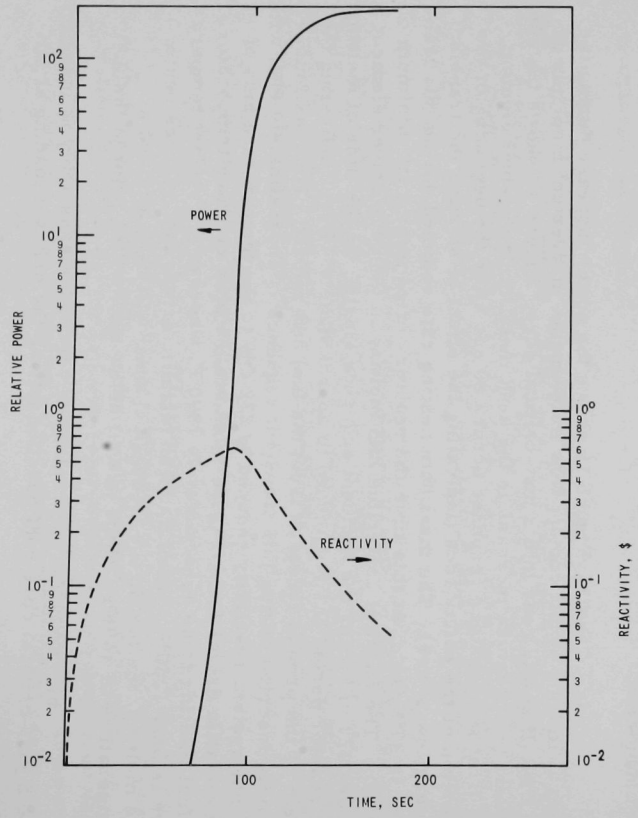

Fig. 16. Power and Reactivity vs Time after Driving Safety Rods into a Just-critical Core at Full Coolant Flow

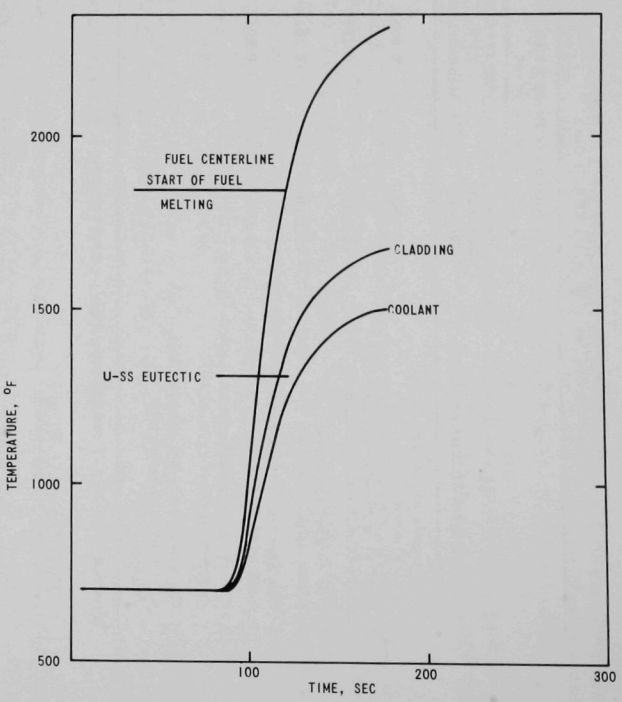

Fig. 17. Peak Fuel-element Temperatures after Driving Safety Rods into a Just-critical Core at Full Coolant Flow

coolant flow. The power burst following this insertion is shown in Fig. 18. Figure 19 indicates the temperature profile in the peak driver-fuel element following the insertion. The first temperature rise occurs approximately 35 sec after the sequence starts. The peak heating rate during this sequence reaches 110°F/sec, and the reactor period goes to a minimum of 0.96 sec. Peak fuel melting at the centerline occurs 49.8 sec after the start of the transient. The reactor period at the point of melting is 13 sec. During the entire transient the maximum system reactivity does not exceed 78¢, and is reduced to 37¢ at the point of fuel melting. Cladding temperature in the peak channel at the point of fuel melting is 1390°F, with the coolant at approximately 1270°F.

The first sign of failure in these first two accidents is either melting in the peak fuel element or formation of uranium-stainless steel eutectic. This would be found to be consistently true in all reactivity incidents studied.

c. Case 3--A single control rod is inserted into a just-critical core during the original loading at full power. The power trace and reactivity history following this inadvertent insertion are presented in Fig. 20. Figure 21 shows the subsequent temperature history of the peak fuel element in the original EBR-II core configuration. As noted, the first sign of temperature rise occurs 120 sec after initiation of the insertion. The maximum heating rate does not exceed 20°F/sec, and the shortest reactor period is 4.5 sec. Centerline melting occurs approximately 220 sec after initiation. At the point of melting, the reactor period has increased to approximately 132 sec. During the entire transient the system reactivity never exceeds 52¢ and is reduced to approximately 10¢ at the point of fuel melting. Cladding temperatures in the transient never exceed 1420°F. The feedback fuel-channel temperature is approximately 1707°F at the point at which the peak fuel element melts.

d. Case 4--A single control rod is assumed to be inserted into a core at 62.5 MWt during the original loading at full coolant flow. Figure 22 shows the power trace following this inadvertent insertion, and Fig. 23 shows that the fuel temperature rises immediately after the insertion. The maximum heating rate during this transient is 13°F/sec, and the shortest reactor period is 97 sec. After 94.5 sec, the first sign of fuel melting occurs in the peak driver-fuel channel. At the point of fuel melting, the reactor period has increased to 122 sec; the system reactivity never exceeds 8.5¢, and at the initiation of fuel melting it has been reduced to 8.2¢.

All the above reactivity incidents are easily prevented by any one of a series of protective-system networks presently installed and operational in EBR-II.

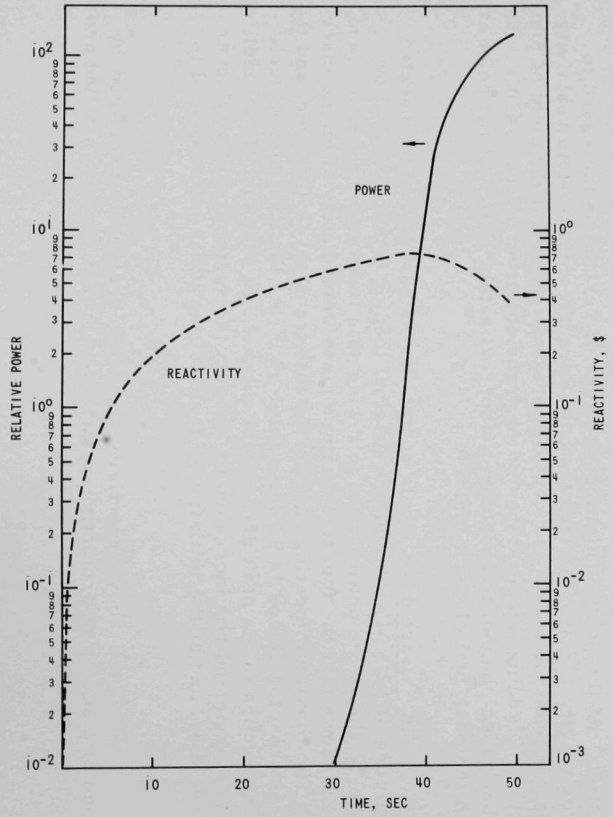

Fig. 18. Power and Reactivity vs Time after Driving One Central Driver-fuel Subassembly into a Just-critical Core at Full Coolant Flow

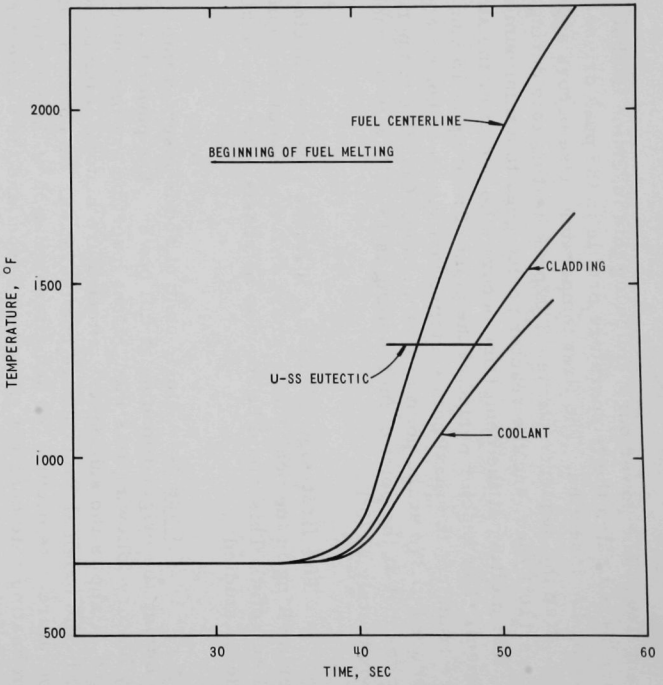

Fig. 19. Peak Fuel-element Temperatures after Driving One Central Driver-fuel Subassembly into a Just-critical Core at Full Coolant Flow

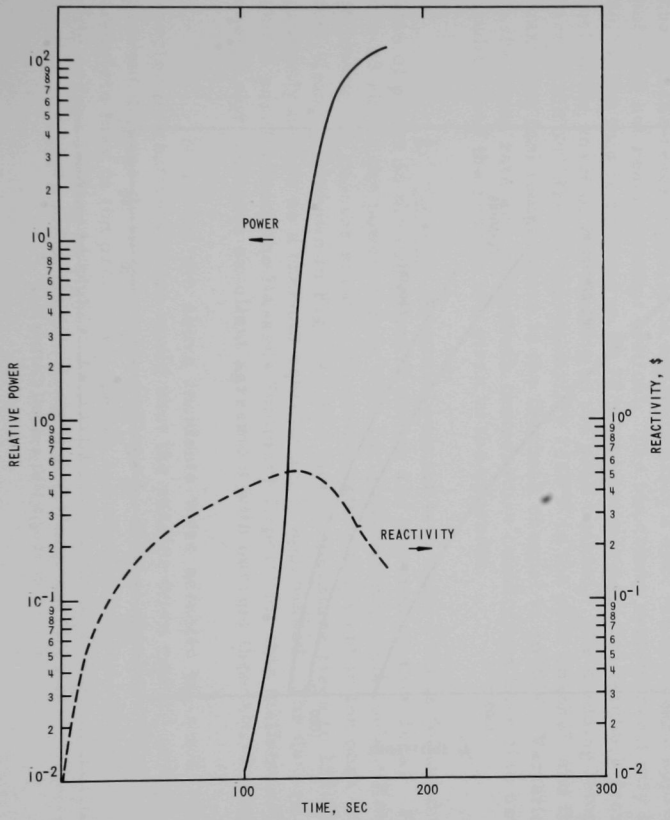

Fig. 20. Power and Reactivity vs Time after Driving One Control Rod into a Just-critical Core at Full Coolant Flow

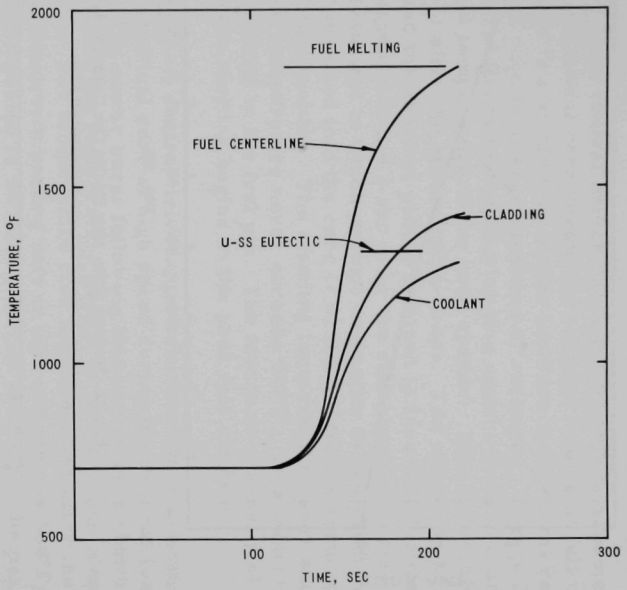

Fig. 21. Peak Fuel-element Temperatures after Driving One Control Rod into a Just-critical Core at Full Coolant Flow

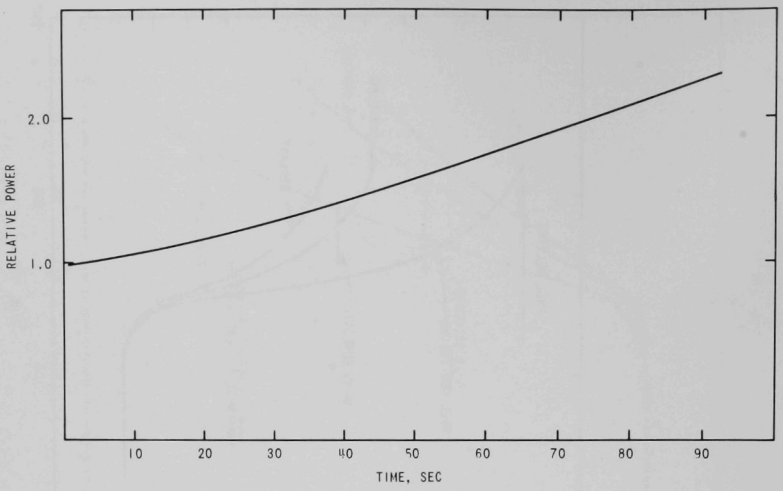

Fig. 22. Power vs Time after Driving One Control Rod into a Core at 62.5 MWt and Full Coolant Flow

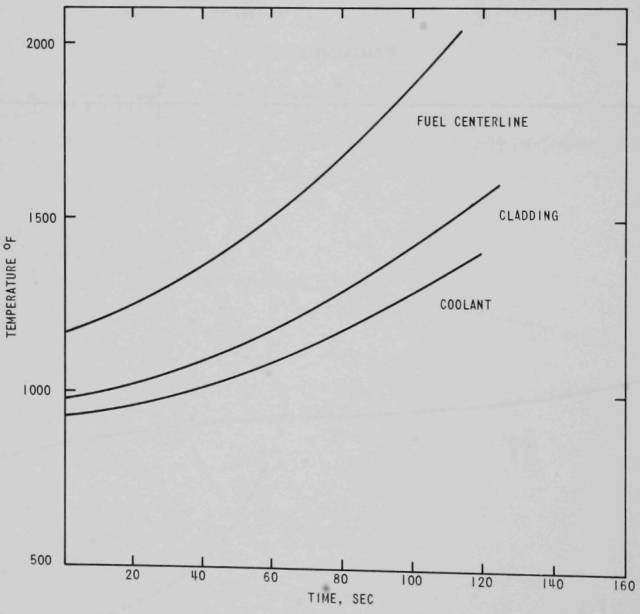

Fig. 23. Peak Fuel-element Temperatures after Driving One Control Rod into a Core at 62.5 MWt and Full Coolant Flow

e. Case 5--A central driver-fuel subassembly is assumed to be dropped into a just-critical core during the original loading at full coolant flow. Although this is a highly improbable incident, it shows the response of the original EBR-II core to a large insertion of reactivity. Figure 24 shows the power and reactivity history during this violent transient, and Fig. 25 shows the fuel temperature in the peak channel. The temperature begins rising 81 msec after the subassembly drops. The maximum heating rate is very large, and the shortest period obtained is less than 0.3 msec. Centerline melting occurs about 0.1 sec after the subassembly drops. This is the only reactor transient in which prompt criticality is achieved. The maximum reactivity inserted into the core is $1.08, but this is reduced to $0.99 at the onset of fuel melting. The cladding temperature never exceeds 864°F, and the coolant temperature never exceeds 797°F. This indicates that all the heat is retained in the fuel pin. The feedback-channel fuel temperature is 1668°F when melting begins in the peak fuel element.

f. Case 6--A central driver-fuel subassembly is assumed to be loaded into a just-critical core at high speed during the original loading at full coolant flow. The power burst following this insertion is shown in Fig. 26. Figure 27 shows the temperature profile in the peak fuel element following the insertion. The temperature rise begins 4.1 sec after the start of the transient. The maximum heating rate in this sequence is 660°F/sec, and the shortest reactor period is 14 msec. At fuel melting in the peak channel the reactor period is approximately 2 sec. This incident approaches, but does not reach, prompt critical. The maximum system reactivity is $0.99, but this is reduced to $0.76 by the prompt negative feedback from the fuel at the onset of fuel melting in the peak channel. The cladding temperature in the accident is approximately 1350°F in the peak channel, and the maximum fuel temperature in the feedback channel is 1670°F. Variations in the ramp rate and in feedback temperature coefficients have also been studied, and the results are given in the appendix.

g. Case 7--A normal reactor trip occurs but is followed by loss of power to the two primary pumps and by primary-flow decay. Figure 28 shows the power versus time (original loading--full coolant flow) following the reactor scram. The temperature transient in the peak driver-fuel element is shown in Fig. 29. The fuel temperature rises to 1300°F and promptly decays as a thermal equilibrium is approached. The dashed curve shows results from the Hazards Summary Report[1] for this malfunction sequence and indicates excellent agreement with current theoretical methods.

If any of the above incidents were actually to occur, the reactor protective system would shut the reactor down rapidly enough to prevent damage in all cases except Case 5. If Case 5 were to occur with complete loss of the protective system and administrative control, along with errors leading to higher-than-expected fuel enrichment, an appreciable amount of core melting would occur. In the complete absence of protection,

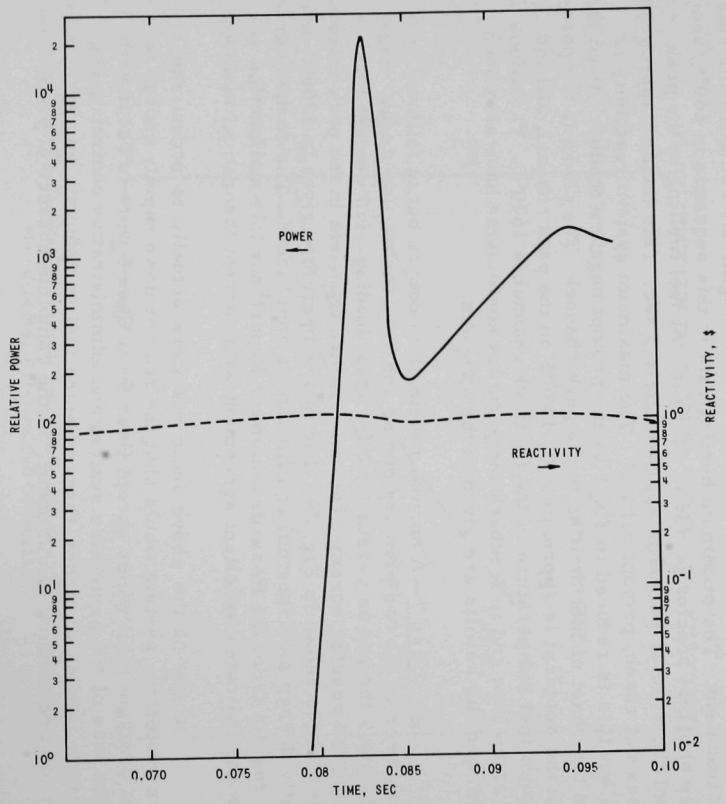

Fig. 24. Power and Reactivity vs Time after Dropping a Central Driver-fuel Subassembly into a Just-critical Core at Full Coolant Flow

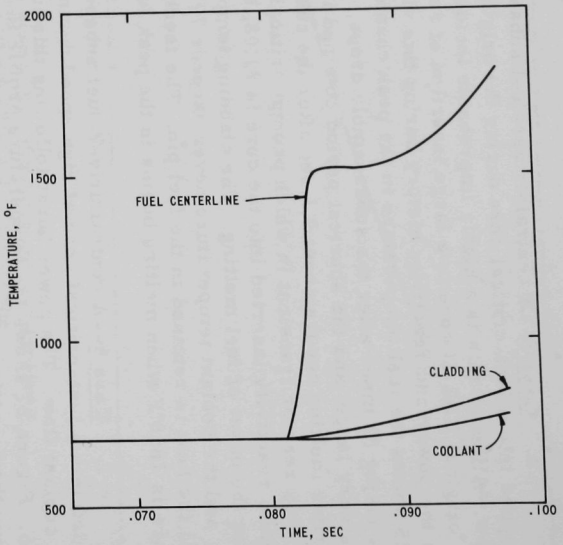

Fig. 25. Peak Fuel-element Temperatures after Dropping a Central Driver-fuel Subassembly into a Just-critical Core at Full Coolant Flow

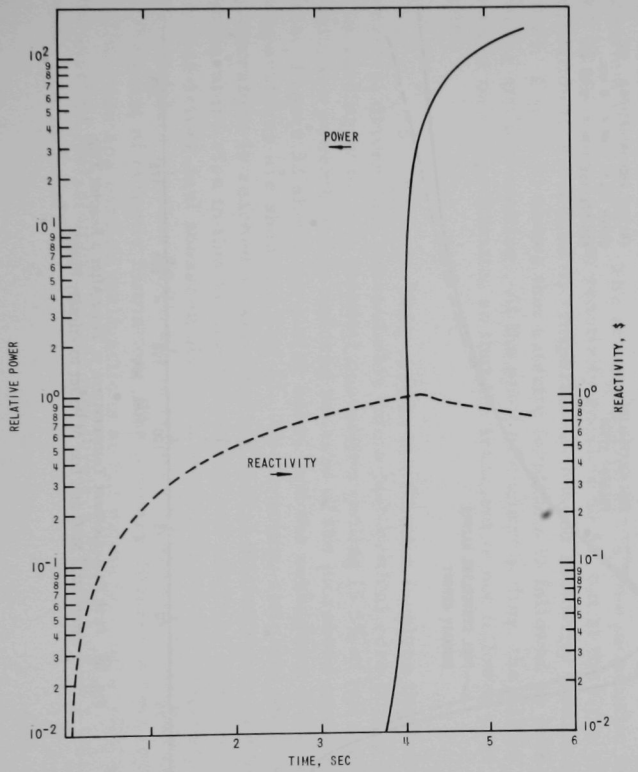

Fig. 26. Power and Reactivity vs Time after Driving a High-speed Central Driver-fuel Subassembly into a Just-critical Core at Full Coolant Flow

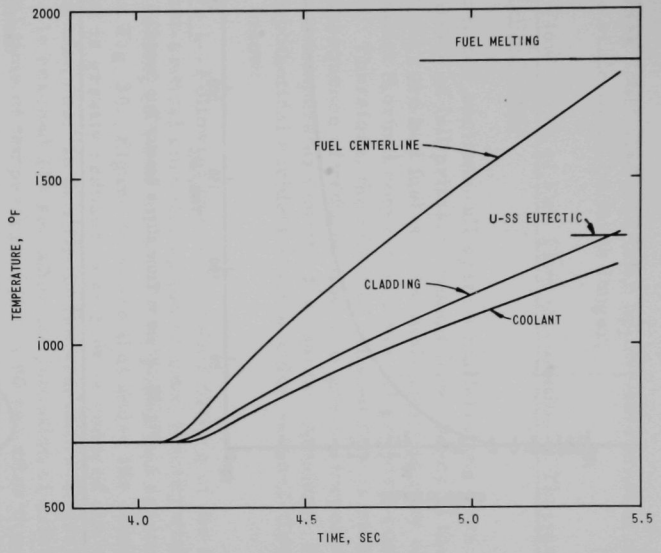

Fig. 27. Peak Fuel-element Temperatures after Driving a High-speed Central Driver-fuel Subassembly into a Just-critical Core at Full Coolant Flow

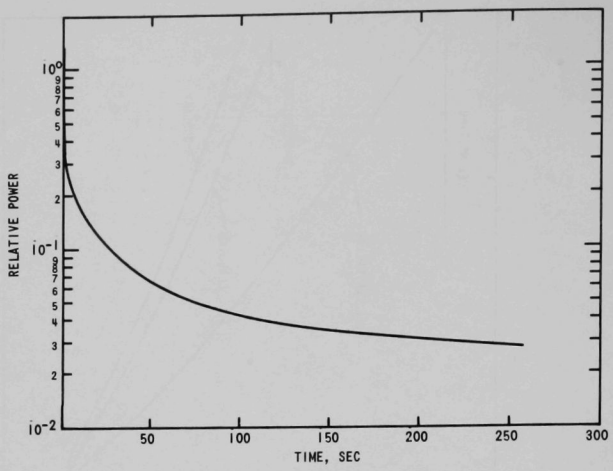

Fig. 28. Power vs Time after a Reactor Trip from 62.5 MWt

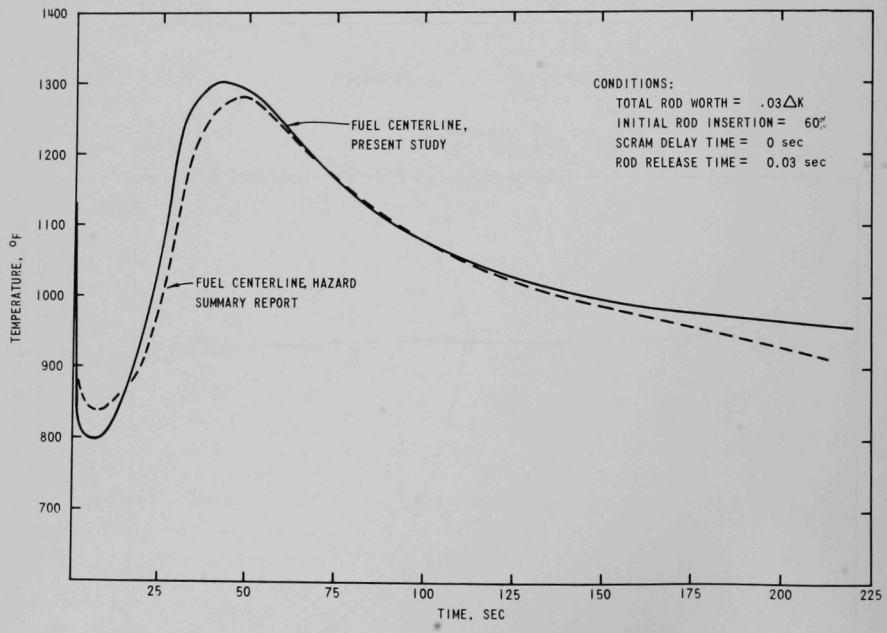

Fig. 29. Peak Fuel-element Temperatures vs Time after a Reactor Trip from 62.5 MWt and Loss of Power to Primary Pumps

some of the other cases could also lead to an appreciable amount of core melting, but the time scale would be much longer.

2. Coolant Flow--5.5% of Full Flow (Simulation of Thermal-convection Cooling)

In the previous sections, all system malfunctions were assumed to occur under conditions of full primary-coolant flow. Many of the cases involving a just-critical core and fuel-subassembly handling may occur only with sodium-coolant thermal convection since all primary-coolant pumps are shut down. Therefore, the effect of reduced flow is studied in this section. The consequence of reduced flow is a greatly increased axial gradient in the coolant temperature during the reactor transient. Results of five of the seven hypothetical accident studies under reduced-flow conditions are presented below:

a. Case 1--Following the uncontrolled driving of the EBR-II safety rods into a just-critical core during the original loading with only thermal convection cooling (5.5% of full flow), the power and reactivity will increase as shown in Fig. 30. Figure 31 shows that under the same conditions the power burst is greatly reduced when flow is reduced due to increased coolant temperatures. In this figure the uranium-stainless steel eutectic temperature is reached 115 sec after the initiation of safety-rod insertion. The initial time of temperature rise is 80 sec after the safety-rod malfunction. The maximum rate of temperature change during this transient is 28°F/sec. The reactor period at the time of eutectic formation is ~70 sec. The system reactivity reaches $0.57, but at the time of eutectic formation it is reduced by temperature-induced reactivity feedbacks to $0.19. Figure 31 shows that eutectic formation is followed by bulk coolant boiling and fuel melting. At the point of coolant boiling, the AIROS model used is only approximate, so that the transient is not followed past this point.

b. Case 2--This system malfunction involves the driving of a central driver-fuel subassembly into a just-critical core during the original loading with only thermal convection cooling (5.5% of full flow). Here again, the power burst is reduced because of the increased coolant temperature. Figure 32 shows the power burst, and the subsequent fuel-element temperatures are shown in Fig. 33. The uranium-stainless steel eutectic temperature is reached 45 sec after the initial malfunction. The initial temperature rise in this accident starts 40 sec after the insertion of the central driver-fuel subassembly. The maximum system reactivity during this transient reaches $0.75, but is reduced by system feedbacks to $0.41 at the point of eutectic formation. The primary difference between a Case-2 malfunction and earlier malfunctions at full primary-coolant flow is that the onset of fuel-element failure now involves cladding failure before centerline fuel melting.

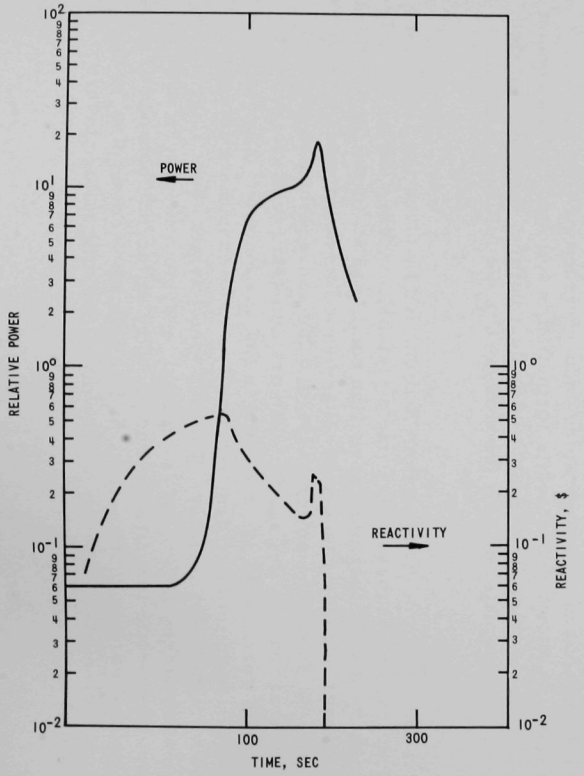

Fig. 30. Power and Reactivity vs Time after Driving Safety Rods into a Just-critical Core at Reduced Coolant Flow

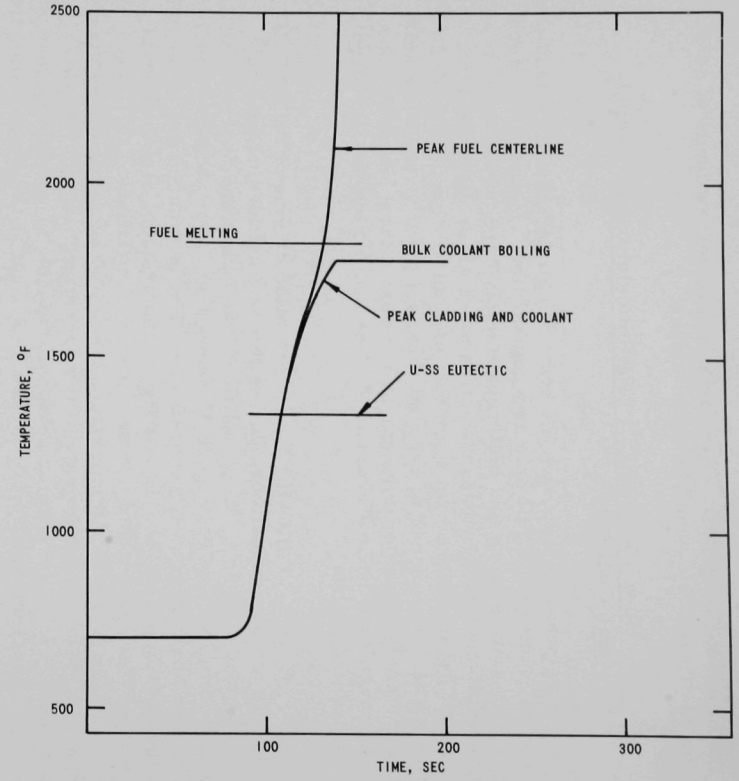

Fig. 31. Peak Fuel-element Temperatures after Driving Safety Rods into a Just-critical Core at Reduced Coolant Flow

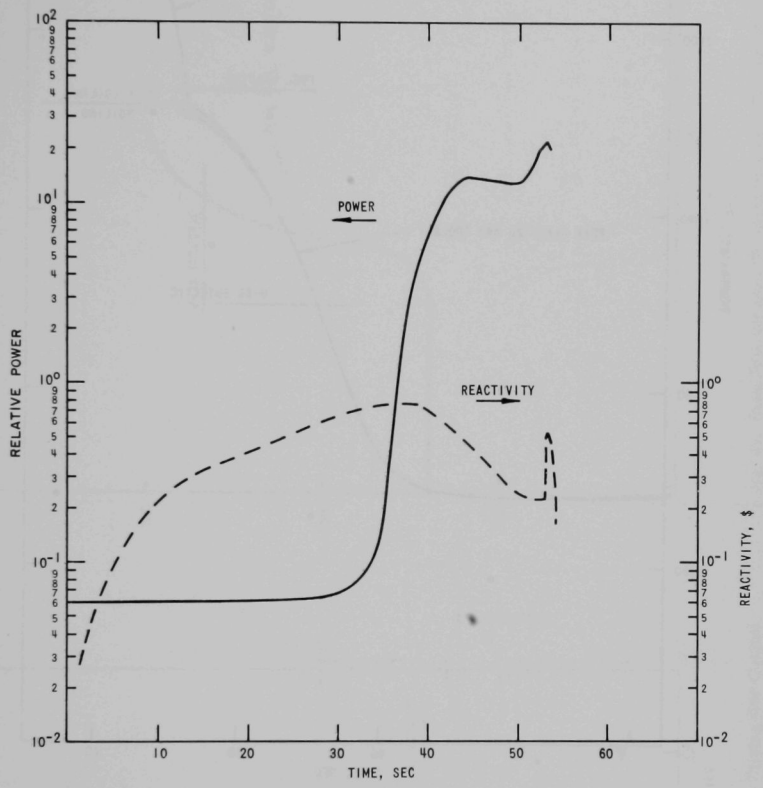

Fig. 32. Power and Reactivity vs Time after Driving the Central Driver-fuel Subassembly into a Just-critical Core at Reduced Coolant Flow

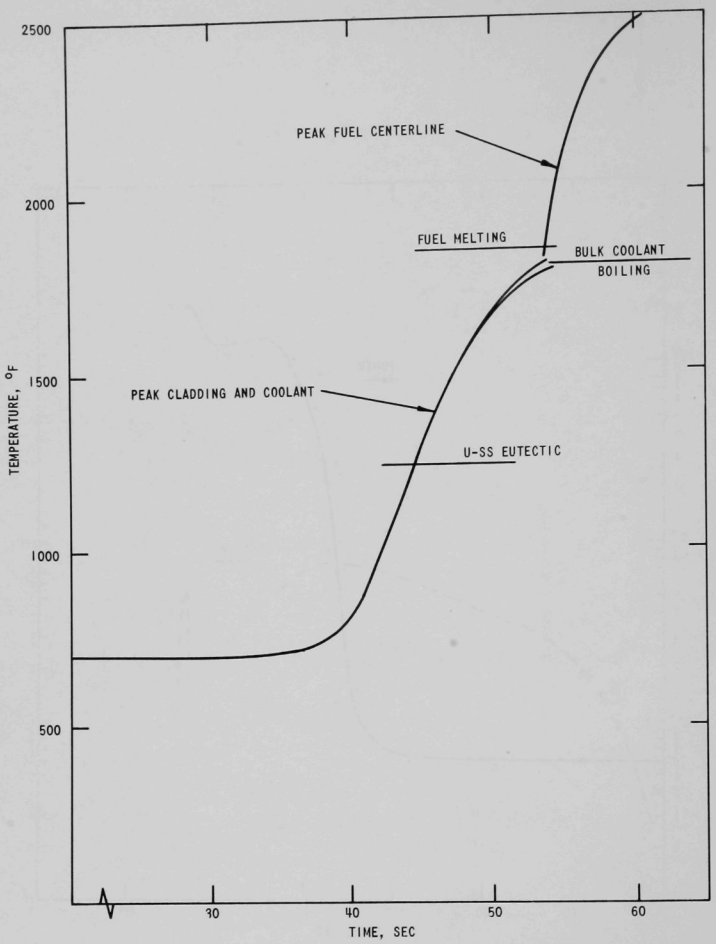

Fig. 33. Peak Fuel-element Temperatures after Driving the Central Driver-fuel Subassembly into a Just-critical Core at Reduced Coolant Flow

c. Case 3--Driving one control rod into a just-critical core (original loading) during reduced coolant flow (5.5% of full flow) produces the power and reactivity distributions shown in Fig. 34; Fig. 35 shows the subsequent fuel-element temperatures following this system malfunction. The uranium-stainless steel eutectic temperature is reached 165 sec after the initiation of the transient. The initial temperature rise, however, occurs 110 sec after the initial insertion of the control rod. The maximum rate of temperature rise in this accident is 15°F/sec, with the shortest period approaching approximately 10 sec. The maximum system reactivity during

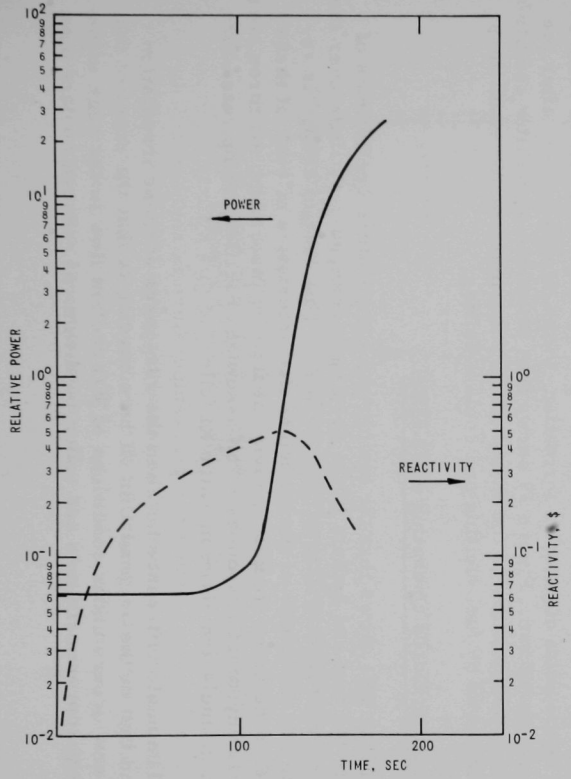

Fig. 34. Power and Reactivity vs Time after Driving One Control Rod into a Just-critical Core at Reduced Coolant Flow

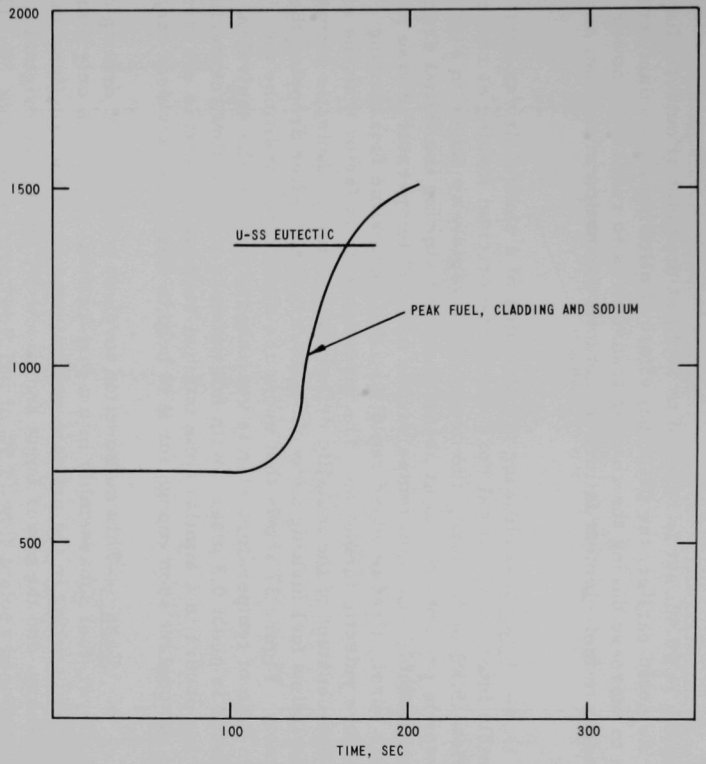

Fig. 35. Peak Fuel-element Temperatures after Driving One Control Rod into a Just-critical Core at Reduced Coolant Flow

this transient is \$0.48, but is reduced to \$0.15 at the point of eutectic formation. As noted earlier, the principal effect of allowing the coolant temperature to increase during the reactor transient is to reduce the power burst leading to fuel-element failure by eutectic formation of the fuel and cladding.

d. Case 5--Following the dropping of a central driver-fuel subassembly into a just-critical core during the original loading at reduced coolant flow (5.5% of full flow), the power rises rapidly as shown in Fig. 36. The reactor is prompt critical at about $7\frac{1}{2}$ msec following the initial drop of the subassembly. Coolant temperatures and fuel temperatures rise rapidly in this burst. Heat is added rapidly so that centerline fuel melting occurs before eutectic formation. The insertion rate is faster than the effective time constant of the metallic driver-fuel element. Eutectic formation would follow fuel melting and would occur 0.15 sec after dropping the subassembly. Figure 37 shows that under the same flow conditions the maximum rate of temperature rise is very sharp, and that the equivalent power period is about 0.3 msec. With full primary-coolant flow, centerline fuel melting occurs in a similar time interval because the heat is not transferred to the coolant soon enough for it to help in this worst accident case.

e. Case 6--This malfunction involves a high-speed driving of a central driver-fuel subassembly into a just-critical core, with only thermal convection cooling in the primary coolant system. This reactivity insertion is sharp, and the power burst and reactivity during the original loading at reduced coolant flow (5.5% of full flow) are noted in Fig. 38. The reactor does not achieve prompt critical, but approaches very closely, with a maximum system reactivity of \$0.99. The system reactivity is reduced to \$0.68 at the point of eutectic formation, which occurs 5.2 sec after the initial high-speed run. Figure 39 shows that under the same flow conditions, the eutectic temperature is the threshold of abnormal reactor conditions. This is followed by fuel melting and coolant boiling.

C. Irradiation Cores Operating at 45 MWt

Table VIII shows that the isothermal temperature coefficients of reactivity for fuel and sodium in the core have changed very little over the various reactor loadings from Runs 16 to 26. This lack of change is reflected in the similarity of the transient characteristics of each of these cores. For the three studies involving reactivity insertions, all three cores had similar dynamic responses. The assumed reactivity ramp rates for Cases 1, 2, and 4 are given in Table XI.

The basic difference between the responses of these irradiation cores and that of the original EBR-II core loading is that the onset of fuel melting now occurs under conditions of full coolant flow in the peak oxide-fuel irradiation experiments and under conditions of reduced coolant flow

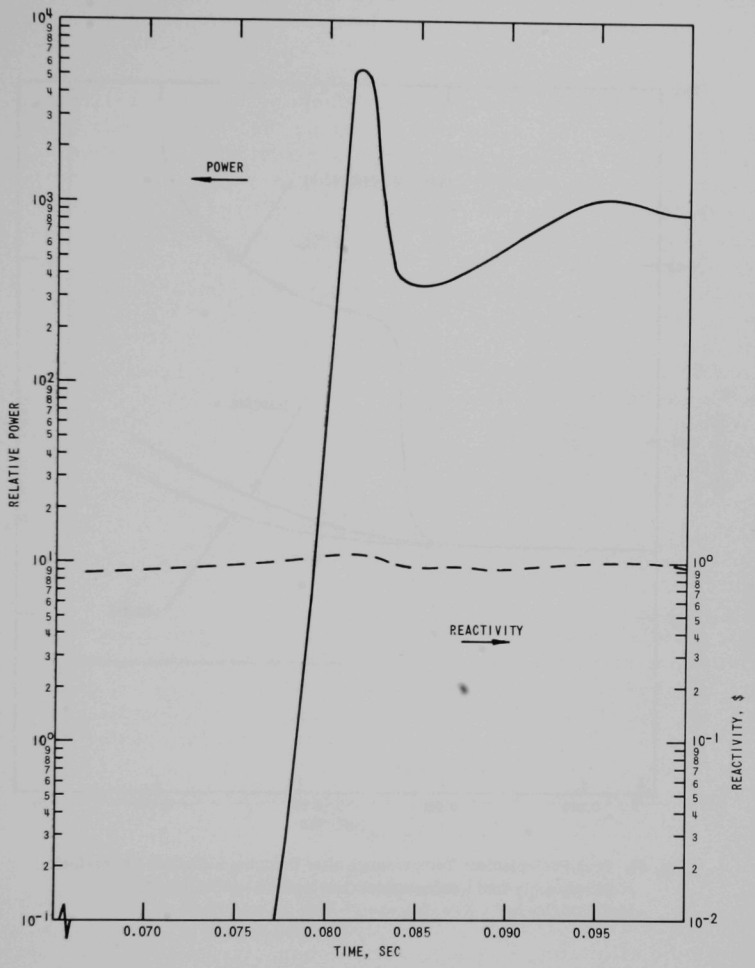

Fig. 36. Power and Reactivity vs Time after Dropping a Central Driver-fuel Subassembly into a Just-critical Core at Reduced Coolant Flow

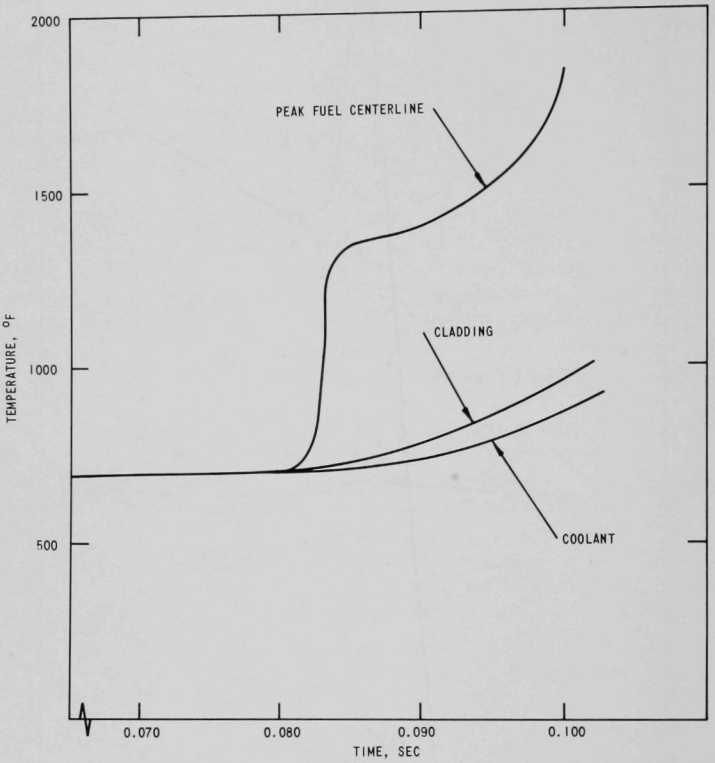

Fig. 37. Peak Fuel-element Temperatures after Dropping a Central Driver-fuel Subassembly into a Just-critical Core at Reduced Coolant Flow

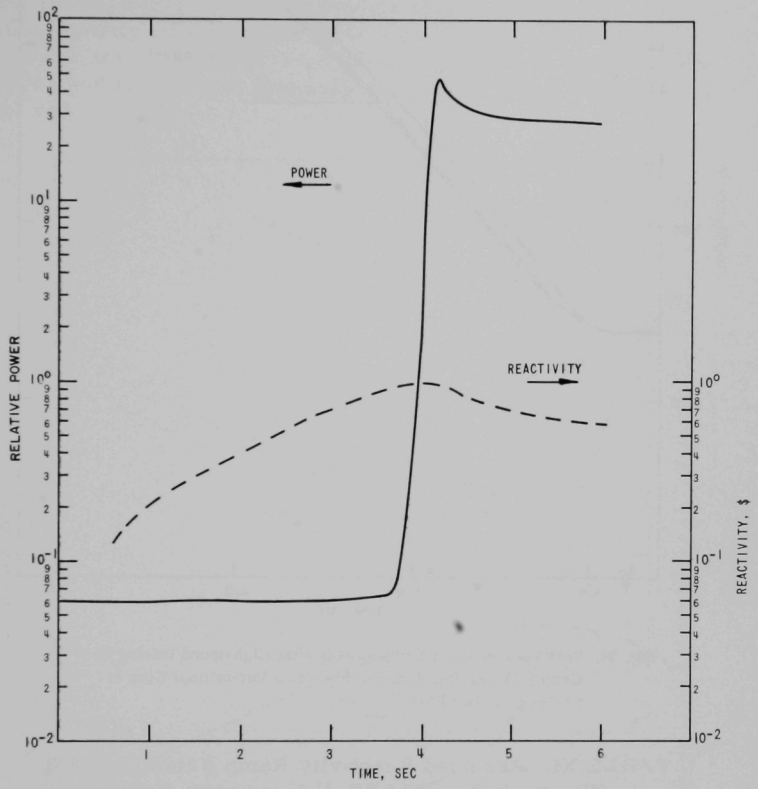

Fig. 38. Power and Reactivity vs Time after Driving a High-speed Central Driver-fuel Subassembly into a Just-critical Core at Reduced Coolant Flow

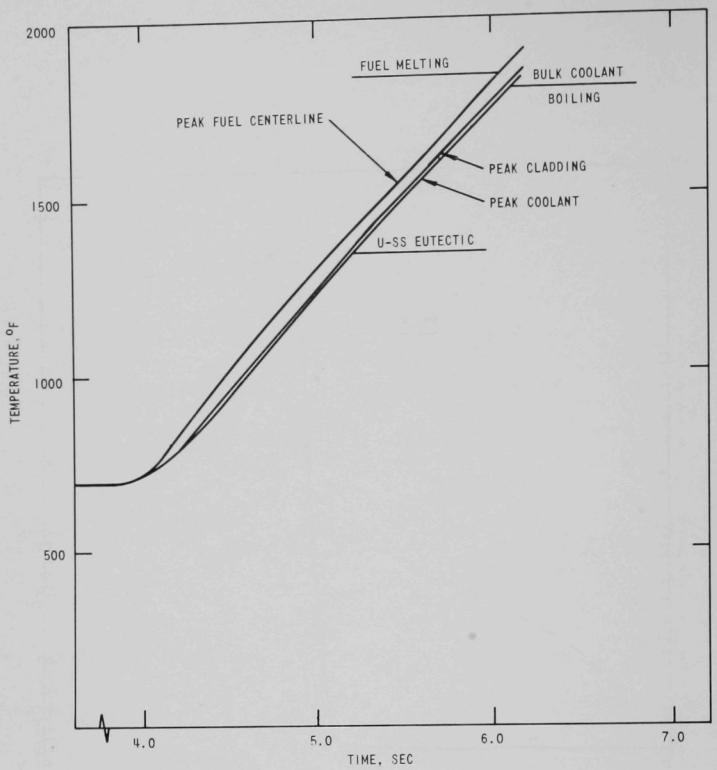

Fig. 39. Peak Fuel-element Temperatures after High-speed Driving of a Central Driver-fuel Subassembly into a Just-critical Core at Reduced Coolant Flow

TABLE XI. Assumed Reactivity Ramp Rates Used for Kinetic Studies of EBR-II Irradiation Cores

Run No.	Safety Rods Just-critical Core, $/sec	Central Subassembly Driven into Just-critical Core, $/sec	One Control Rod Driven into Core at 45 MWt, $/sec
16, 24, 26	0.0033	0.0146	0.0028

in the metallic driver-fuel elements. Figures 40 and 41 show the power traces and temperature characteristics of the three irradiation cores (Runs 16, 24, and 26) following an accidental insertion of the safety rods into a just-critical core during full coolant flow. Figures 42 and 43 present the power and reactivity histories and subsequent temperature profiles of Runs 16, 24, and 26 following the accidental insertion of a central driver-fuel subassembly into a just-critical core during full coolant flow. Figure 44 presents the temperature profiles of the same three runs in a reactor core at 45 MWt and full coolant flow following the accidental insertion of a control rod.

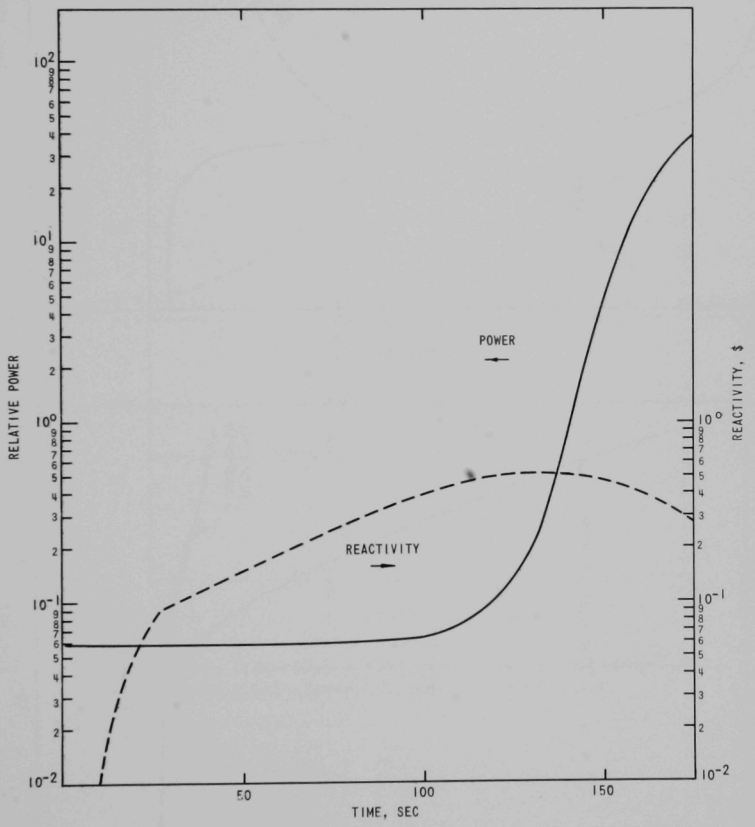

Fig. 40. Power and Reactivity Increase after Driving Safety Rods into a Just-critical Core at Full Coolant Flow

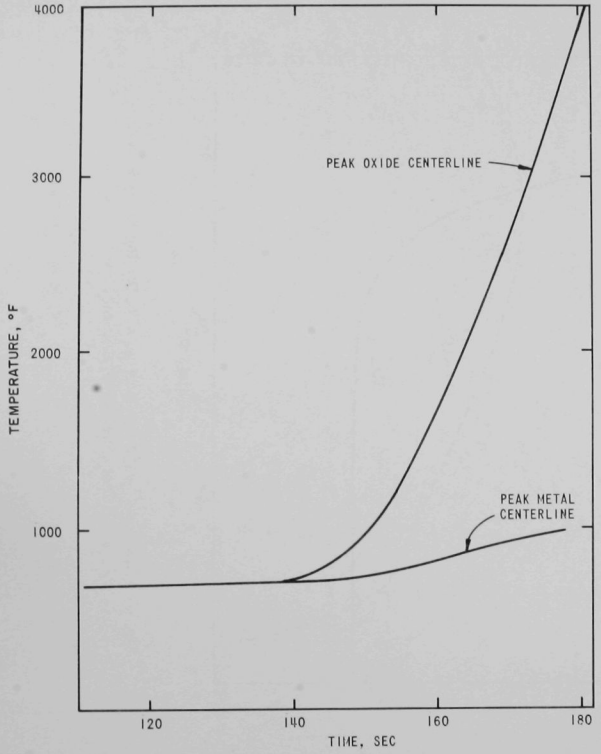

Fig. 41. Peak Fuel Temperatures vs Time after Driving Safety Rods into a Just-critical Core at Full Coolant Flow

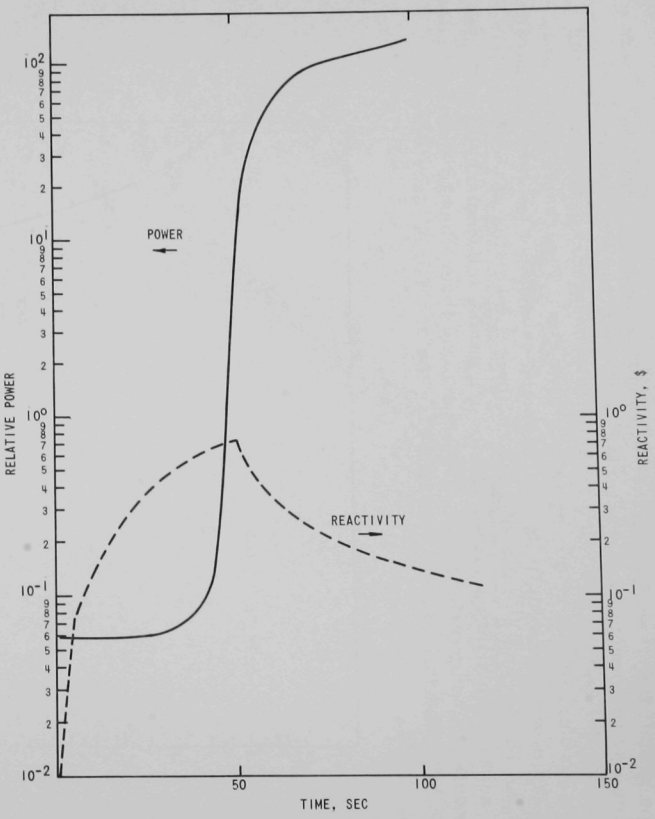

Fig. 42. Power and Reactivity vs Time after Driving a Central Fuel Subassembly into a Just-critical Core at Full Coolant Flow

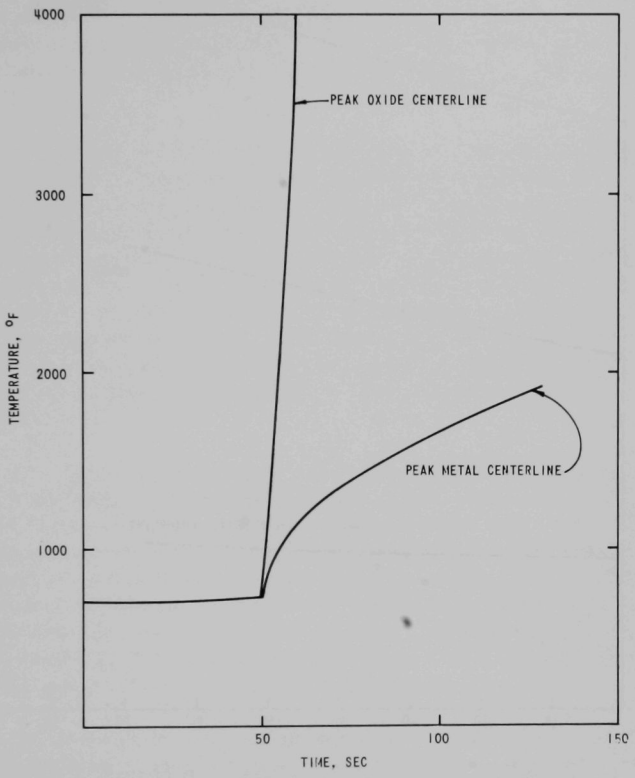

Fig. 43. Peak Fuel Temperatures vs Time after Driving a Central Driver-fuel Subassembly into a Just-critical Core at Full Coolant Flow

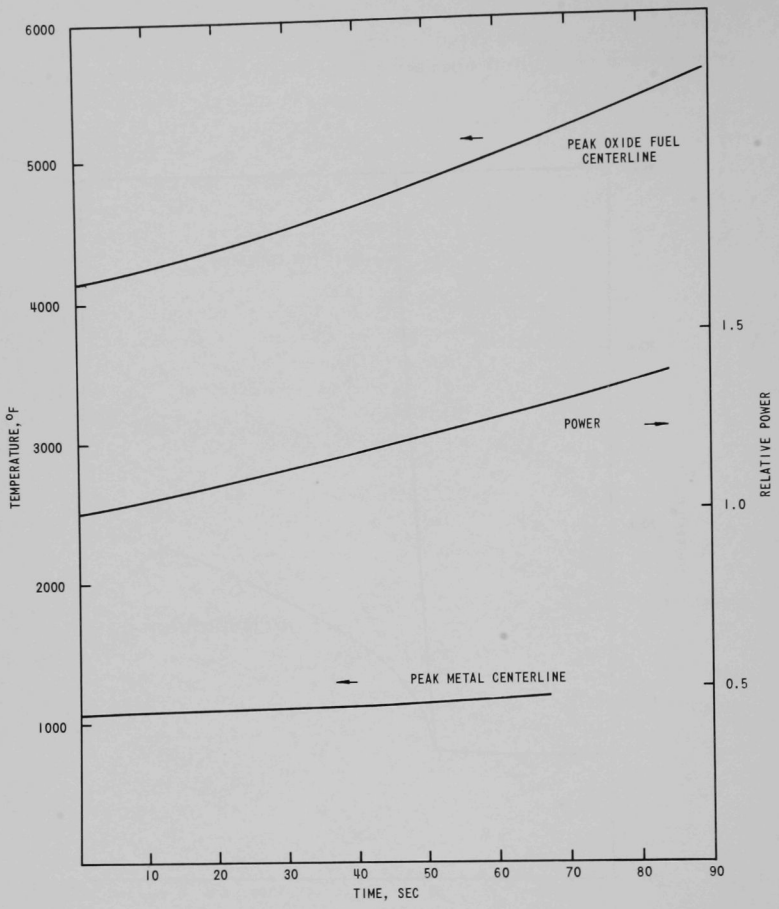

Fig. 44. Peak Fuel Temperatures and Power vs Time after Driving One Control Rod into a Core at 45 MWt and Full Coolant Flow

1. Full Coolant Flow

Under full-coolant-flow conditions, only three of the seven hypothetical malfunction cases (Cases 1, 2, and 4) are considered.

a. Case 1--Following the inadvertent insertion of the safety rods into a just-critical core, the first sign of temperature rise occurred after 140 sec. The maximum rate of temperature rise in the oxide fuel was 113°F/sec, and the minimum reactor period was 5.4 sec. Fuel melting occurred in the peak oxide-fuel pin 190 sec after the start of the accident

sequence. The oxide fuel melted before the metallic fuel because of its higher power generation and operating temperature, and the lower thermal conductivity (as compared to metallic-fuel elements). The reactor period at the point of fuel melting was 59 sec. The peak reactivity inserted in this accident sequence was 49¢, and this was reduced to approximately 22¢ at the onset of melting in the oxide pin. Figure 41 shows that the peak metallic driver-fuel temperature did not exceed 1000°F, because of its lower power generation and operating temperature, and higher thermal conductivity.

b. Case 2--A central driver-fuel subassembly is inserted into a just-critical core. The first sign of oxide-fuel temperature rise in all three core configurations considered occurred at approximately 50 sec. The maximum rate of temperature rise in the oxide fuel pin was 300°F/sec. The shortest period achieved in this incident was 1.35 sec. Melting in the oxide-fuel pin occurred approximately 62 sec after the start of the malfunction sequence. At the point of fuel melting, the reactor period had increased to approximately 33 sec. The maximum reactivity during this sequence never exceeded 73¢ and was reduced to 34¢ at the point of fuel melting, because of the prompt negative feedback from the metallic driver subassemblies.

c. Case 4--A control rod is assumed to be inserted after the reactor is at 45 MWt. A temperature rise in the oxide pin occurs immediately after the inadvertent insertion of the control rod. The maximum rate of temperature rise in the oxide during this sequence was 125°F/sec. The shortest reactor period during the transient was 222 sec. Centerline-fuel melting in the oxide pin occurred 65 sec after the start of the accident sequence. The reactor period had increased to approximately 226 sec at the point of fuel melting. The maximum reactivity insertion and also the reactivity at the point of fuel melting was approximately 4¢.

No attempt is made in this report to characterize the volume of oxide fuel melting during a hypothetical transient. Instead, the onset of failure in the oxide pins was taken as the terminal point in these initial review studies of the dynamic response of EBR-II.

2. Coolant Flow--5.5% of Full Flow (Simulation of Thermal-convection Cooling)

Under reduced coolant flow (5.5% of full flow) only two of the original seven hypothetical malfunction cases are considered. The behavior of past irradiation cores is dramatically different in the case where only thermal-convection cooling is assumed during a system malfunction. In the studies above in which full primary coolant flow was assumed, the experimental oxide fuel melted before any driver-fuel temperature reached levels of concern. With the primary pumps off and only thermal-convection

cooling present, formation of the uranium-stainless steel eutectic occurs before the experimental oxide-fuel centerline temperature reaches the melting point. The main reason for this is that now the coolant temperature rises very rapidly and gives a sharp negative reactivity feedback that limits the power burst and thereby protects the oxide-fuel experiments; however, there is potential for gross formation of uranium-stainless steel eutectic in driver-fuel subassemblies. Only Cases 1 and 2 are considered.

a. Case 1--Following the driving of safety rods into a just-critical core (Runs 16, 24, and 26) containing experimental oxide subassemblies and metallic driver fuel, and with only thermal coolant-convection cooling (5.5% of full flow), the power and reactivity burst that follows are shown in Fig. 45. Figure 46 shows the resulting metallic driver-fuel element temperatures and peak oxide centerline temperature. Formation of uranium-stainless steel eutectic occurs in about 115 sec. At this point, the peak oxide centerline temperature is 1740°F. The main cause of the lowering of the peak oxide centerline temperature is the prompt negative feedback due now to rise in temperature of the fuel and coolant in a situation where only auxiliary coolant flow removes the transient heat.

b. Case 2--This model involves driving a central driver-fuel subassembly into a just-critical core (Runs 16, 24, and 26) containing oxide fuel experiments, metallic driver fuel, and only auxiliary-pump coolant flow (5.5% of full flow). The power and reactivity burst (shown in Fig. 47) is reduced due to the prompt negative feedback from the driver-fuel and sodium-coolant temperature rise in the reactor core. Figure 48 shows the peak fuel-element temperatures for Runs 16, 24, and 26 at reduced coolant flow following the initiation of this malfunction. Formation of uranium-stainless steel eutectic is reached in approximately 46 sec, and the centerline temperature of the peak oxide is approximately 1680°F. Again the prompt rise in the temperatures of the driver-fuel and sodium coolant limit the power burst protecting the oxide fuel experiments, but leads to the formation of a uranium-stainless steel eutectic in the driver-fuel element.

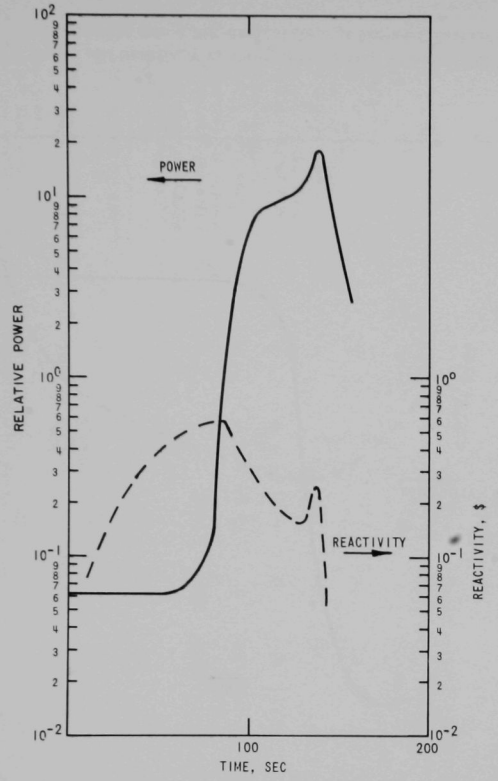

Fig. 45. Power and Reactivity vs Time after Driving Safety Rods into a Just-critical Core at Reduced Coolant Flow

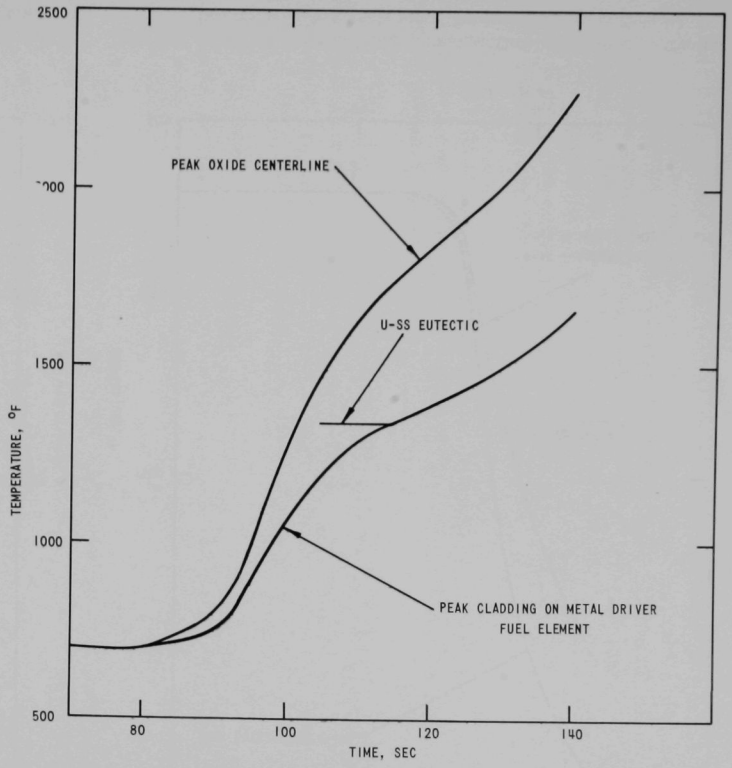

Fig. 46. Peak Fuel-element Temperatures vs Time after Driving Safety Rods into a Just-critical Core at Reduced Coolant Flow

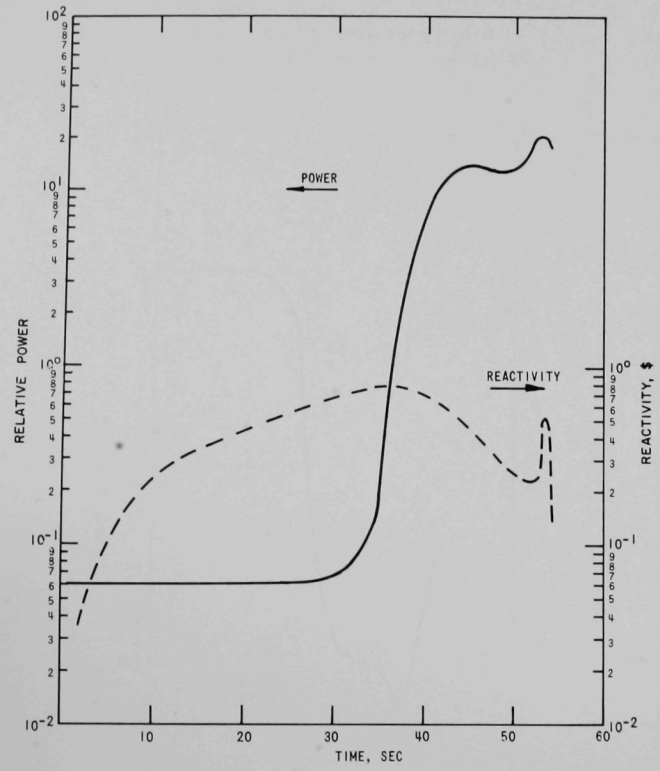

Fig. 47. Power and Reactivity vs Time after Driving a Central Driver-fuel Subassembly into a Just-critical Core at Reduced Coolant Flow

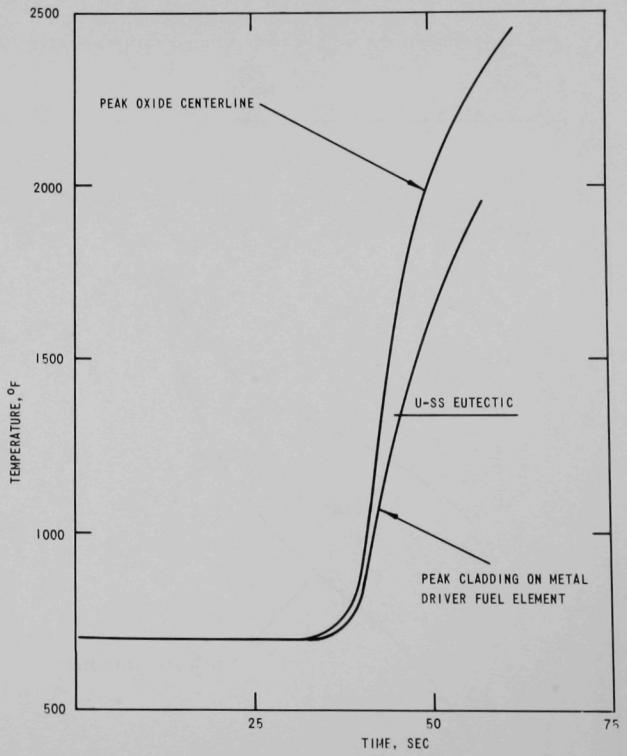

Fig. 48. Peak Fuel-element Temperatures vs Time after Driving a Central Driver-fuel Subassembly into a Just-critical Core at Reduced Coolant Flow

V. SUMMARY AND CONCLUSIONS

A summary of the calculated dynamic responses under full-coolant-flow conditions of a variety of EBR-II core configurations is presented in Table XII. Six of the seven hypothetical reactivity incidents were considered in reviewing the dynamic response of the original EBR-II core. In subsequent irradiation cores three accident sequences were studied, and the basic conclusions drawn are:

(1) In the original EBR-II core loading, all reactivity incidents considered can be averted by action of the control and protective system, and by administrative control.

(2) A sequence most probably leading to severe consequences in the EBR-II is the dropping of a central fuel subassembly into a just-critical core, along with a series of malfunctions or maloperations in the control and protective system, and complete loss of administrative control.

(3) The dynamic responses of various irradiation cores (Runs 16-24) are quite similar because the temperature coefficients of reactivity for each core have not changed significantly from the earlier characteristics of the EBR-II core loadings.

(4) The main difference between the dynamic response of the original EBR-II core and the later irradiation configuration is that the first

TABLE XII. Summary of Calculated Dynamic Responses of a Variety of EBR-II Core Configurations (Assuming 100% Coolant Flow)

Case No.	Accident Simulation	Time to Initial Temp. Rise, sec		Temperature Transient in Fuel: Maximum Rate of Temp. Rise, °F/sec	Temperature Transient in Fuel: Shortest Reactor Period, sec	Time to Centerline Melting of Fuel, sec	Reactor Period at Melting, sec	System Reactivity, $: Maximum	System Reactivity, $: At Time of Fuel Melting
1.	Safety rods driven into just-critical core--original loading	≈80	Metallic Fuel Driver	37	2.92	121	44	0.598	0.23
2.	Central driver-fuel subassembly driven into just-critical core--original loading	≈35		110	0.96	49.8	13	0.772	0.37
3.	One control rod driven into just-critical core--original loading	≈120		20	4.5	220	132	0.518	0.100
4.	One control rod driven into core 62.5 MWt--original loading	≈0		13	97	94.5	122	0.0849	0.082
5.	Central driver-fuel subassembly dropped into just-critical core--original loading	0.081		234×10^3	0.00028	0.0982	-0.012	1.075	0.985
6.	Central driver-fuel subassembly driven at high speed into just-critical core--original loading	4.1		650	0.0141	515	2	0.994	0.760
1.	Safety rods driven into just-critical core--Runs 16, 24, 26	140	Experimental Fuel Oxide	113	5.4	190	59	0.486	0.760
2.	Central driver-fuel subassembly driven into just-critical core--Runs 16, 24, 26	50		300	1.35	62	33	0.752	0.343
3.	One control rod driven into core at 45 MWt, Runs 16, 24, 26	≈0		125	222	65	226	0.04	0.040

point of concern for fuel temperatures would occur in the oxide-fuel irradiation experiments under conditions of full coolant flow. In the case of reduced coolant flow, the first points of concern are the driver-fuel temperatures.

(5) As the number of irradiation experiments is increased, a more detailed analysis of the temperature profiles, reactivity coefficients, and dynamic responses of ceramic-fueled irradiation experiments is required to assess their influence on the overall core kinetics of EBR-II.

(6) Under full-coolant-flow conditions the peak oxide-fuel elements undergo melting before the peak metallic elements. Therefore, initial core fuel melting will be noncoherent. Initial melting of an oxide-fuel element, however, would tend to reinforce the ramp insertion of reactivity in the core that initiated the excursion. Thus the rate of heating of the metallic (mostly driver) fuel would be reinforced. This would also result in earlier action by protective circuits (period and power-level trips), would tend to obviate the more catastrophic consequences which may be postulated, but might also tend to accelerate some defecting of driver fuel.

APPENDIX A

Theoretical Reactor Modeling

Figure 49 shows the reduced power-to-reactivity feedback network used in these studies. A two-channel, heat-transfer model was used for kinetic studies of the original EBR-II core, and a five-channel heat-transfer model was used to study subsequent irradiation cores (see Figs. 14 and 15).

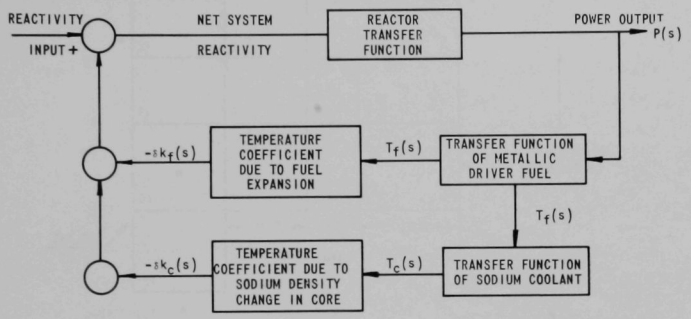

Fig. 49. Reduced Power-to-Reactivity EBR-II Feedback Network

1. Temperature

The basic AIROS-IIA heat-transfer model used in these studies is seen in Fig. 50 (see Ref. 3 for details), where i is the index for the axial heat-transfer nodes and j the index for the radial heat-transfer nodes. Neglecting axial conduction, the heat-balance equations for this model are:

a. Noncoolant Nodes

$$(\rho C_p V)_{ij} T_{ij}(t) = H_{ij} N(t) + UA_{i,j-1}[T_{i,j-1}(t) - T_{i,j}(t)] + UA_{i,j}[T_{i,j+1}(t) - T_{i,j}(t)] \quad (1)$$

b. Outlet Temperature Model: Coolant Node

$$T_{i,j}(t) = \theta_j(t), \quad (2)$$

where

T = temperature;

j = radial-node index;

i = axial-node index;

θ = inlet temperature;

$H_{i,j}$ = the volumetric heat-generation rate;

$UA_{i,j}$ = the overall heat-transfer coefficient across the right-hand boundary of node (i,j);

$(\rho C_p V)$ = the density, specific heat, and volume of node (i,j).

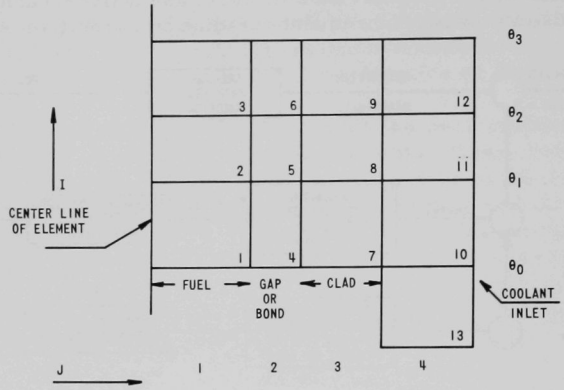

Fig. 50. Schematic Representation of the AIROS-IIA Heat-transfer Model

2. Reactivity

The net system reactivity is obtained in AIROS-IIA from the equation

$$r(t) = r(o) + \min(t_1, \gamma_4) + \sum_{j=i}^{NF} A_j \delta T_j(t); \qquad t \leq (t_s + t_D), \tag{3}$$

where

$r(o)$ = initial reactivity in \$;

γ_1 = rate of linear reactivity insertion (\$/sec);

γ_4 = maximum reactivity insertion (\$);

NF = number of feedback equations;

t_s = time (sec at which reactor trip signal is sensed);

t_D = delay time (sec) between time reactor trip signal is sensed and reactor trip;

$A_j = \frac{\delta k}{\delta T_j}$ = the temperature coefficient of reactivity.

Thus the reactivity feedback in each accident sequence is computed by the integral

$$\delta k_j = \int_{T_j(o)}^{T_j(t)} \left(\frac{\delta r}{\delta T_j}\right) dT_j. \qquad (4)$$

The variations in reactor power are obtained by solving the standard space-independent neutron equations for prompt and delayed precursors.[3]

APPENDIX B

Dynamic Response Data (Survey Cases)

Table XIII summarizes the AIROS-IIA parametric kinetic studies of transient cases for the original EBR-II core loading.

TABLE XIII. AIROS-IIA Parametric Results for Kinetic Studies of the Original EBR-II Core Loading

(Assuming 100% coolant flow)

Case No.	Type of Problem	Time to Melting, sec	Relative Power	Reactivity, $	Main Variable	Peak Channel		Feedback Channel		
						Cladding Temp, °F	Coolant Temp, °F	Fuel Temp, °F	Cladding Temp, °F	Coolant Temp, °F
1-0	Safety rods driven into just-critical core: γ_1 = \$0.0067/sec; α_f = -0.288×10^{-3} \$°F; α_c = -0.644×10^{-3}	121 (120)[a]	135	0.23	γ_1	1392	1260	1690	1553	1436
1-1	Safety rods driven into just-critical core: γ_1 = \$0.0033/sec; α_f = -0.288×10^{-3}; α_c = -0.644×10^{-3}	202	≈100	≈0.17	γ_1	1440	1260			
1-2	Safety rods driven into just-critical core: γ_1 = \$0.0067/sec; α_f = -0.148×10^{-3}; α_c = -0.322×10^{-3}	106	133	≈0.425	α_f, α_c	1386	1261	1674	1535	1425
1-3	Safety rods driven into just-critical core: γ_1 = \$0.0033/sec; α_f = -0.148×10^{-3}; α_c = -0.322×10^{-3}	178	131	≈0.310	γ_1, α_f, α_c	1388	1263	1674	1540	1430
2-0	Central fuel subassembly driven into just-critical core: γ_1 = \$0.02/sec; α_f = -0.288×10^{-3}; α_c = -0.644×10^{-3}	49.8 (55)[a]	130	0.37	γ_1	1390	1270	1680	1544	1434
2-1	Central fuel subassembly driven into just-critical core: γ_1 = 0.0146; α_f = -0.288×10^{-3}; α_c = -0.644×10^{-3}	64	≈130	≈0.37	γ_1	1388	1263	1674	1539	1428
2-2	Central fuel subassembly driven into just-critical core: γ_1 = \$0.02/sec; α_f = -0.148×10^{-3}; α_c = -0.322×10^{-3}	44	≈139	0.60	α_f, α_c	1367	1255	1672	1515	1409
2-3	Central fuel subassembly driven into just-critical core: γ_1 = 0.0146; α_f = -0.148×10^{-3}; α_c = -0.322×10^{-3}	57.4	≈136	≈0	γ_1, α_f, α_c	≈1378	≈1255	≈1668	≈1519	≈1412
3-1	One control rod driven into just-critical core: γ_1 = \$0.004/sec; α_f = -0.288×10^{-3}; α_c = -0.644×10^{-3}	220 ≈(230)[a]	≈120	≈0.10	γ_1	1420	1280	≈1707	≈1558	≈1430
3-2	One control rod driven into just-critical core: γ_1 = \$0.004/sec; α_f = -0.148×10^{-3}; α_c = -0.322×10^{-3}	155	132	+0.34	α_f, α_c	1388	1262	1674	≈1538	1428
4-0	One control rod driven into core at 62.5 MWt: γ_1 = \$0.004/sec; α_f = -0.288×10^{-3}; α_c = -0.644×10^{-3}	94.5 (40-80)[a] (20-40)[a]	2.35	0.082	γ_1	≈1390	≈1265	≈1595	≈1476	≈1374
4-1	One control rod driven into core at 62.5 MWt: γ_1 = \$0.0028/sec; α_f = -0.288×10^{-3}; α_c = -0.322×10^{-3}	130	2.35	0.063	γ_1	1390	1265	1595		≈1374
4-2	One control rod driven into core at 62.5 MWt: γ_1 = \$0.004/sec; α_f = -0.148×10^{-3}; α_c = -0.322×10^{-3}	67.4	2.35	0.1175	α_f, α_c	1390	1265	1595	1447	1374
4-3	One control rod driven into core at 62.5 MWt: γ_1 = \$0.0028/sec; α_f = -0.148×10^{-3}; α_c = -0.322×10^{-3}	90.0	2.35	0.0964	γ_1, α_f, α_c	1390	1265	1595	1447	1324
5-0	Central fuel subassembly dropped into just-critical core: γ_1 = \$13.2/sec; α_f = -0.288×10^{-3}; α_c = -0.644×10^{-3}	0.0982 (≤0.13)[a]	1130	0.985	γ_1	≈864	≈797	1668	≈909	≈824
5-1	Central fuel subassembly dropped into just-critical core: γ_1 = \$5.6/sec; α_f = -0.288×10^{-3}; α_c = -0.644×10^{-3}	0.248	495	0.966	γ_1	1058	989	≈1638	≈1113	≈1048
5-2	Central fuel subassembly dropped into just-critical core: γ_1 = \$13.2/sec; α_f = -0.148×10^{-3}; α_c = -0.644×10^{-3}	0.0831	36454	0.966	α_f, α_c	707	704	1702	710	706
5-3	Central fuel subassembly dropped in just-critical core: γ_1 = \$5.6/sec; α_f = -0.148×10^{-3}; α_c = -0.644×10^{-3}	0.230	636	0.978	γ_1, α_f, α_c	866	791	1650	915	820
6-0	Central fuel subassembly driven at high speed into just-critical core: γ_1 = \$0.241/sec; α_f = -0.288×10^{-3}; α_c = -0.644×10^{-3}	5.5 (≈6.0)[a]	150	0.76	γ_1	1350	1270	≈1670	≈1483	≈1420
6-2	Central fuel subassembly driven at high speed into just-critical core: γ_1 = \$0.24/sec; α_f = -0.148×10^{-3}; α_c = -0.322×10^{-3}	4.85	≈172	≈0.84	α_f, α_c	≈1326	≈1220	≈1663	≈1433	≈1347
6-3	Central fuel subassembly driven at high speed into just-critical core: γ_1 = \$0.24/sec; α_f = -0.148×10^{-3}; α_c = -0.644×10^{-3}	5.1	≈157	≈0.80	α_f	≈1355	≈1230	≈1673	≈1481	≈1384

[a]Values presented in Hazard Summary Report (ANL-5719 and Addendum).

Two basic variations were studied for most of these cases:

(1) reduced reactivity ramp rate to correspond with measured reactivity, and

(2) reduced prompt negative feedback to study the effect of loss of fuel expansion, large cores, etc.

1. Reduced Reactivity Ramp Rate

Under reduced reactivity ramp rate only six of the original seven hypothetical malfunction cases (and variations thereof) were considered.

In Case 1-0 (Table XIII) the time required to melt driver fuel in the peak channel was 120 sec for normal prompt feedback and a ramp rate of \$0.0067/sec. Reducing the ramp rate by 50% to \$0.0033/sec (Case 1-1) increased the time to melting by less than a factor of two (202 sec). Reducing the prompt feedback from fuel and sodium by 50% (Case 1-2) reduced the time to melting by only about 12% (106 sec). Finally, reducing both the ramp rate and prompt feedback by 50% (Case 1-3) increased the time to melting by 50% (178 sec). The major effect in Case 1-0 was clearly the imposed reactivity ramp rate. Figure 51 shows the power and reactivity versus time for Case 1-1 (normal feedback and 50% reduction in ramp rate), and Fig. 52 shows the associated temperatures for Case 1-1.

Similar results were obtained for a Case-2 malfunction. Figure 53 shows the temperatures following the driving of a central fuel subassembly into a just-critical core (Case 2-1; reduced ramp rate and normal prompt feedback). Figures 54 and 55 show the power, reactivity, and peak temperatures for the same transient but with a reduction in prompt feedback as well as ramp rate.

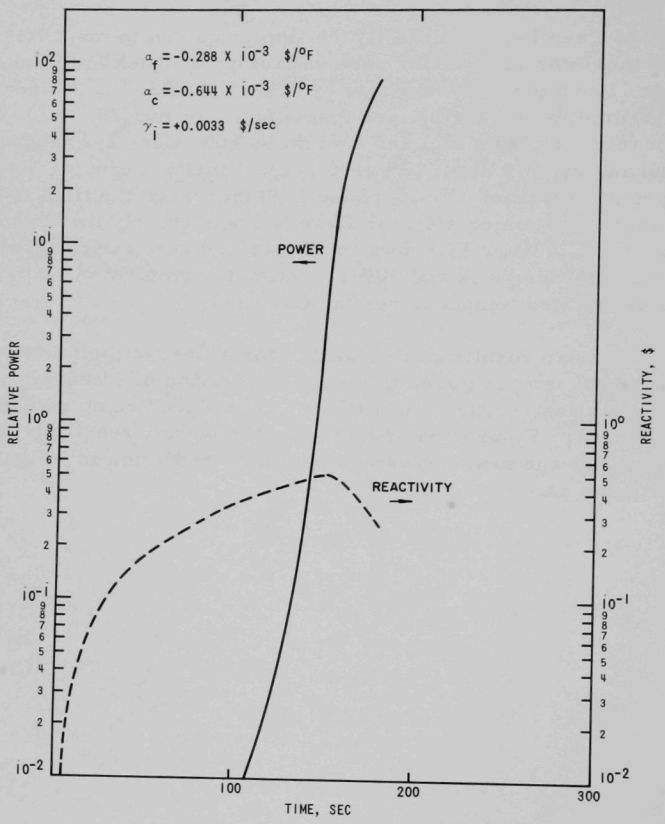

Fig. 51. Power and Reactivity vs Time after Driving Safety Rods into a Just-critical Core at Full Coolant Flow

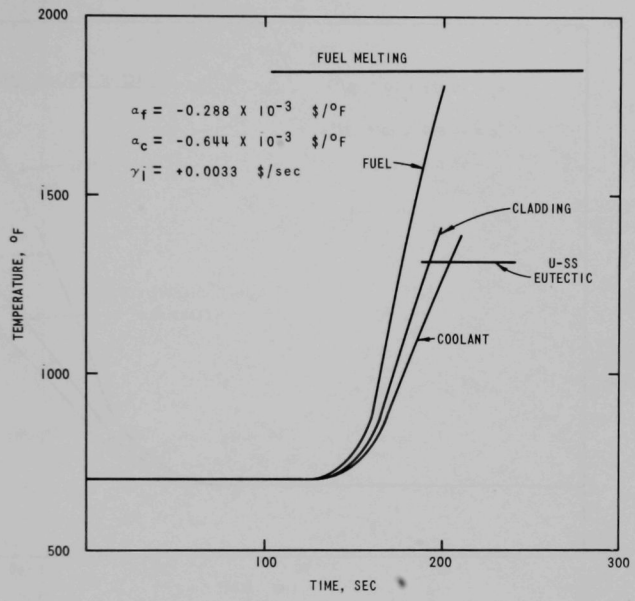

Fig. 52. Peak Fuel-element Temperatures after Driving Safety Rods into a Just-critical Core at Full Coolant Flow

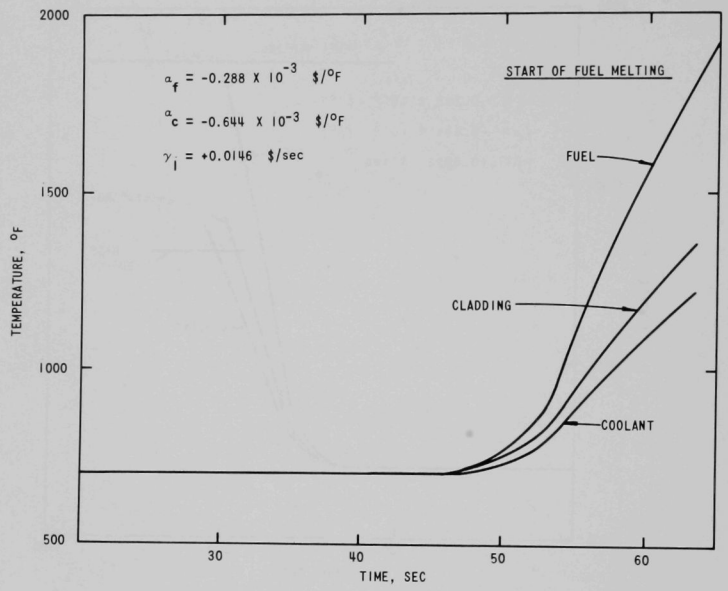

Fig. 53. Peak Fuel-element Temperatures after Driving a Central Driver-fuel Subassembly into a Just-critical Core at Full Coolant Flow

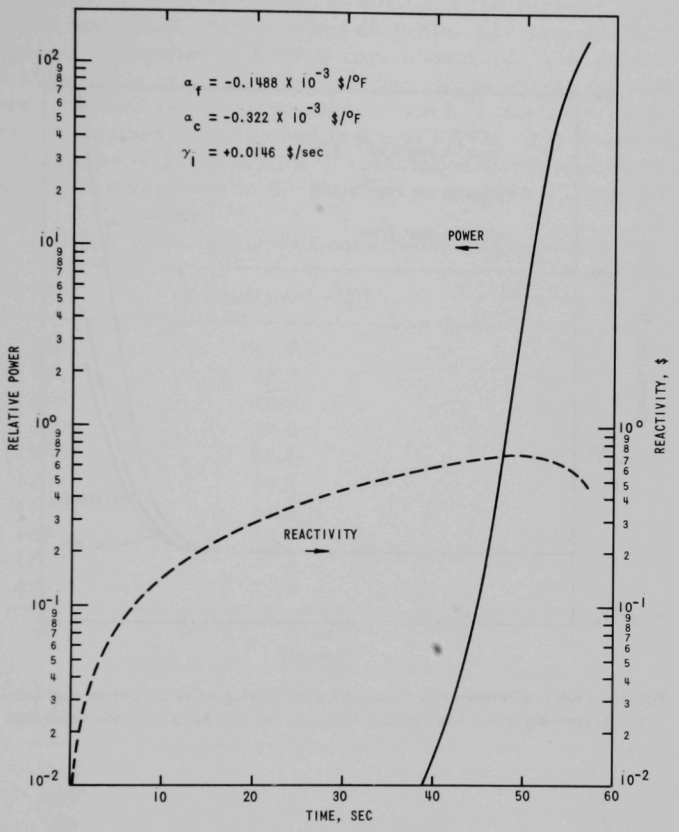

Fig. 54. Power and Reactivity vs Time after Driving a Central Driver-fuel Subassembly into a Just-critical Core with Reduced Ramp Rate and Feedbacks

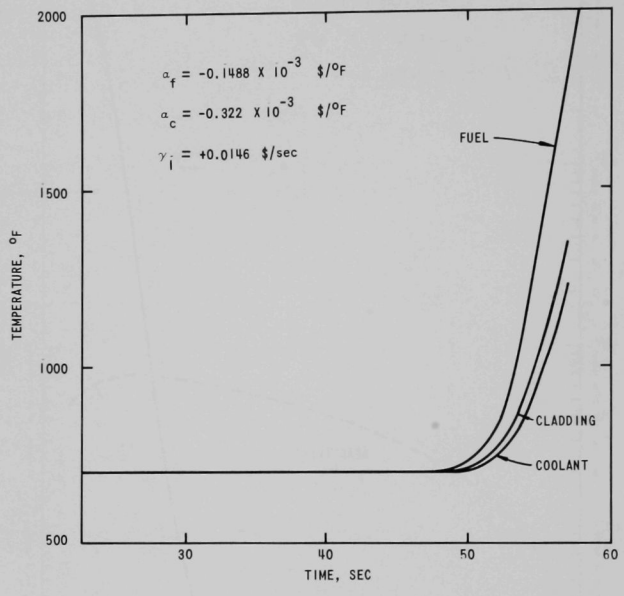

Fig. 55. Peak Fuel-element Temperatures after Driving a Central Driver-fuel Subassembly into a Just-critical Core with Reduced Ramp Rate and Feedbacks

APPENDIX C

Physical Properties of Core Materials

References 9-12 were used to establish the physical properties of EBR-II core materials. Summarized in Tables XIV through XXVI are the basic physical properties of EBR-II core materials. The AIROS-IIA program does not allow for a change in physical properties during the transient. Therefore, constant values were used for each of the basic physical properties; these values are summarized in Table XXVII. Future studies of the dynamic response of present EBR-II irradiation cores will include some variation with temperature in the physical properties of core materials.

TABLE XIV. Thermal Conductivity of Liquid Sodium

T, °F	k (Btu/hr-ft-°F)	k (Btu/sec-ft-°F)
600	43.8	0.01217
700	42.2	0.01172
800	40.5	0.01125
900	39.0	0.01080
1000	37.6	0.01044
1200	34.7	0.00964
1400	32.1	0.00891
1600	29.6	0.00822
1800	27.4	0.00761
2000	25.0	0.00694

TABLE XV. Density of Liquid Sodium

T, °F	ρ, lb/ft^3	T, °F	ρ, lb/ft^3
400	56.4	1200	49.7
600	54.7	1400	48.0
700	53.8	1600	46.5
800	53.1	1800	44.8
900	52.2	2000	43.0
1000	51.4		

TABLE XVI. Viscosity of Liquid Sodium

T, °F	η, lb$_m$/ft-hr	η, lb$_m$/ft-sec	T, °F	η, lb$_m$/ft-hr	η, lb$_m$/ft-sec
400	1.05	2.92×10^{-4}	1000	0.50	1.42×10^{-4}
600	0.78	2.16	1200	0.44	1.22
700	0.68	1.89	1400	0.42	1.16
800	0.61	1.69	1600	0.40	1.11
900	0.55	1.52			

TABLE XVII. Specific Heat of Liquid Sodium

T, °F	C_p, Btu/lb-°F	T, °F	C_p, Btu/lb-°F
200	0.330	1000	0.300
400	0.320	1200	0.300
600	0.312	1400	0.301
700	0.308	1600	0.305
800	0.305		

TABLE XVIII. Thermal Conductivity of Stainless Steel

T, °F	k, Btu/hr-ft-°F	k, Btu/sec-ft-°F	T, °F	k, Btu/hr-ft-°F	k, Btu/sec-ft-°F
200	8.20	0.00228	900	11.30	0.00314
400	9.10	0.00253	1000	11.70	0.00325
600	10.00	0.00278	1200	12.60	0.00350
700	10.40	0.00289	1400	13.40	0.00372
800	10.80	0.00300	1600	14.3	0.00397

TABLE XIX. Specific Heat of Stainless Steel

T, °F	C_p, Btu/lb-°F
400	0.123
600	0.129
700	0.132
800	0.135
900	0.138
1000	0.140
1200	0.144
1400	0.148
1600	0.152
1800	0.154

TABLE XX. Density of Stainless Steel

T, °F	ρ, lb/ft^3
400	493.0
600	490.0
700	488.0
800	486.6
900	485.0
1000	483.0
1200	480.0
1400	476.5
1600	473.0
1800	469.5

TABLE XXI. Thermal Conductivity of Uranium-5 wt % Fissium Alloy

T, °C	T, °F	k, cal/sec-cm-°C	k, Btu/sec-ft-°F
100	212	0.048	0.003225
200	392	0.052	0.003494
250	482	0.055	0.003695
300	572	0.059	0.003964
350	662	0.061	0.004098
400	752	0.065	0.004367
500	932	0.072	0.004837
550	1022	0.077	0.005173
600	1112	0.083	0.005577
650	1202	0.086	0.005778
700	1292	0.093	0.006249
750	1382	0.102	0.006854

TABLE XXII. Specific Heat of Uranium-5 wt % Fissium Alloy

ΔH cal	T, °F	C_p, Btu/lb-°F
	$\alpha + \delta + U_2Ru$	
5.3	200	0.0265
3.0	300	0.0300
3.1	400	0.0310
4.2	500	0.0420
3.6	560	0.0600

ΔH cal	T, °C	C_p, Btu/lb-°F
	$\alpha + \delta - U_2Ru$	
5.8	200	0.0290
3.5	300	0.035
3.7	400	0.037
4.4	500	0.044
4.6	600	0.046

ΔH cal	T, °C	C_p, Btu/lb-°F
	γ and $\gamma + U_2Ru$	
5.8	200	0.0290
3.5	300	0.035
3.7	400	0.037
4.4	500	0.044
-	560	
-	560	
4.6	600	0.046
-	640	
-	640	
4.7	700	0.047
-	750	
4.1	800	0.041
4.9	900	0.049
5.9	1000	0.059

TABLE XXIII. Density of Uranium-Fissium Alloy

wt % Fissium	ρ, g/cc	ρ, lb/ft³
3	18.4-18.50	1150-1159
4	18.1-18.30	1130-1140
5	17.9-18.20	1120-1139
6	17.80-18.10	1110-1130
7	17.7-17.9	1105-1120

TABLE XXIV. Specific Heat of UO_2

T, °C	T, °F	C_p, Btu/lb-°F
100	212	0.063
200	392	0.067
500	932	0.074
1000	1832	0.078
1500	2732	0.082

TABLE XXV. Variation of Thermal Conductivity of UO_2 with Bulk Density

ρ, g/cc	k, W/cm-°C	k, Btu/sec-ft-°F	ρ, g/cc	k, W/cm-°C	k, Btu/sec-ft-°F
8.4	0.048	0.0007707	9.6	0.060	0.0009634
9.0	0.055	0.0008831	9.8	0.062	0.0009955
9.2	0.057	0.0009152	10.0	0.064	0.001027
9.4	0.0585	0.0009393	10.8	0.070	0.0011239

TABLE XXVI. Thermal Conductivity of $(0.2\ Pu\text{-}0.8\ U)O_{2.04}$

(ρ = 93.1% T.D)

T, °C	T, °F	k, W/cm-°C	k, Btu/sec-ft-°F	T, °C	T, °F	k, W/cm-°C	k, Btu/sec-ft-°F
855	1571	0.0196	0.0003147	1325	2417	0.0205	0.0003211
911	1671	0.0203	0.0003259	1334	2433	0.0200	0.0003211
919	1686	0.0216	0.0003468	1384	2523	0.0209	0.0003356
924	1695	0.0204	0.0003275	1375	2507	0.0216	0.0003468
1011	1851	0.0219	0.0003516	1514	2757	0.0225	0.0003613
1061	1941	0.0229	0.0003677	1523	2773	0.0235	0.0003773
1200	2192	0.0157	0.0002521	1533	2791	0.0225	0.0003613

TABLE XXVII. Assumed Physical Properties for Initial Review of the EBR-II Dynamic Response

Core Material	Equivalent Temperature, °F	Density, lb/ft^3	Conductivity, Btu/sec-ft-°F	Specific Heat, Btu/lb-°F	Viscosity, lb/sec-ft
Sodium coolant	1000	51.4	0.01044	0.300	1.42×10^{-4}
Stainless steel, Type 304	1000	483	0.00350	0.140	-
Uranium-5 wt % Fissium	1100	1120	0.00550	0.046	-
PuO_2-UO_2	2800	640	0.00036	0.080	-

APPENDIX D

EBR-II Design and Operating Data

Table XXVIII summarizes the major physical properties of the EBR-II power plant as originally presented in the Hazards Summary Report,[1,2] ANL-5719 and Addendum.

TABLE XXVIII. Summary of EBR-II Design and Operating Data[2]

General	
Heat output, MW	62.5
Gross electrical output, MW	20
Primary sodium temperature, to reactor, °F	700
Primary sodium temperature, from reactor, °F	883
Primary sodium flow rate, through reactor, gpm	9,000
Primary sodium maximum velocity, in core, fps	23.8
Primary system sodium capacity, gal	89,000
Secondary sodium temperature, to heat exchanger, °F	588
Secondary sodium temperature, from heat exchanger, °F	866
Secondary sodium flow rate, gpm	5,890
Steam generator	
Output, lb/hr	250,000
Steam temperature, °F	837
Steam pressure, psig	1,300
Feed-water temperature, °F	550
Turbine throttle conditions	
Steam flow, lb/hr	195,300
Steam temperature, °F	837
Steam pressure, psig	1,250
Reactor Data (67-Subassembly Core)	
Core dimensions	
Equivalent diameter, in.	19.94
Height, in.	14.22
Total volume, liter	72.79
Upper and lower blanket dimensions	
Equivalent diameter, in.	19.94
Length (each end), in.	18.0
Inner-blanket dimensions	
Equivalent OD, in.	27.46
Length, in.	55.0
Radial thickness, in.	3.76
Outer-blanket dimensions	
Equivalent OD, in.	61.5
Length, in.	55.0
Radial thickness, in.	17.02
Core composition	
Fuel alloy, vol %	31.8
Stainless steel (Type 304), vol %	19.5
Sodium, vol %	48.7

TABLE XXVIII (Contd.)

Reactor Data (Contd.)	
Control and safety-rod composition (fuel section)	
Fuel alloy, vol %	21.3
Stainless steel (Type 304), vol %	21.5
Sodium, vol %	57.2
Upper and Lower Blanket Composition	
Uranium (depleted), vol %	30.3
Stainless steel (Type 304), vol %	18.5
Sodium, vol %	51.2
Inner-blanket Composition	
Uranium, vol %	60.0
Stainless steel (Type 304), vol %	19.6
Sodium, vol %	20.4
Outer-blanket Composition	
Uranium (depleted), vol %	60.0
Stainless steel (Type 304), vol %	20.9
Sodium, vol %	19.1
Subassemblies	
Core	53
Control (rod and thimble)	12
Safety (rod and thimble)	2
Inner blanket	60
Outer blanket	510
Total	637
Configuration	Hexagonal
Dimension across flats, in.	2.290
Hexagonal tube thickness, in.	0.040
Structural material	304 SST
Lattice spacing (pitch), in.	2.320
Clearance between subassemblies, in.	0.030
Fuel Elements (Pin-type, Sodium Bonded)	
Fuel pin chamber, in.	0.144
Fuel pin length, in.	14.22
Fuel tube	0.174
Fuel tube wall thickness, in.	0.009
Thickness of sodium bond annulus, in.	0.006
Elements per subassembly	91
Upper and Lower Blanket Elements (Pin-type, Sodium Bonded)	
Blanket pin diameter, in.	0.3165
Blanket pin length (total), in.	18.0
Blanket tube, OD, in.	0.376
Blanket tube wall thickness, in.	0.022
Thickness of sodium-bond annulus, in.	0.008
Blanket elements per subassembly (each end)	18
Control and Safety Rods	
Configuration	Hexagonal

TABLE XXVIII (Contd.)

Control and Safety Rods (Contd.)	
Dimension across flats, in.	1.908
Fuel elements	Same as core subassembly
Fuel elements per rod	61
Inner and Outer Blanket Elements (Pin-type, Sodium Bonded)	
Blanket pin diameter, in.	0.433
Blanket pin length (total), in.	55.0
Blanket tube OD, in.	0.493
Blanket tube wall thickness, in.	0.018
Thickness of sodium bond annulus, in.	0.012
Blanket elements per subassembly	19
Fuel Alloy (Enriched Uranium-Fissium)	
Total core loading, kg	385
U-235 enrichment, at. %	48.4
Critical mass--U-235 (clean, full power), kg	172
Total mass of U-235 in core, kg	176
Fuel Alloy Composition (Fissium)	
Uranium, wt %	95.0
Zirconium, wt %	0.06
Molybdenum, wt %	2.48
Ruthenium, wt %	1.97
Rhodium, wt %	0.29
Palladium, wt %	0.19
Niobium, wt %	0.01
Fertile Blanket Material (Depleted Uranium)	
Total blanket loading, kg	28,100
Nuclear Data	
Total fissions cc/sec at center of core	3.7×10^{13}
Neutron energy distribution at center of core	
Flux above 1.35 MeV, n/cm^2-sec	0.69×10^{15}
Flux below 1.35 MeV, n/cm^2-sec	2.86×10^{15}
Total neutron flux, n/cm^2-sec	3.55×10^{15}
Prompt neutron lifetime, sec	8×10^{-8}
Reactor Control	
Full-flow power coefficients	
0-62.5 MW (no bowing), $(\Delta k/k)/MW$	-3.5×10^{-5}
0-25 MW (with bowing), $(\Delta k/k)/MW$	-3.5×10^{-5}
25-34 MW (with bowing), $(\Delta k/k)/MW$	$+1.0 \times 10^{-5}$
34-62.5 MW (with bowing), $(\Delta k/k)/MW$	-4.0×10^{-5}
Doppler effect--average $(\Delta k/k)/°C$	$< +0.04 \times 10^{-5}$
Isothermal temperature coefficient $(\Delta k/k)/°C$	-3.6×10^{-5}
Total reactivity worth	
12 normal control rods, $\Delta k/k$	0.048
2 safety rods, $\Delta k/k$	0.013

TABLE XXVIII (Contd.)

Reactor Control (Contd.)	
Control rod	
Total	12
Operating drive (each rod)	Rack and pinion
Velocity, in./min	5
Total movements, in.	14.0
Scram drive	Pneumatic
Safety rod	
Total	2
Operating drive	Rack and pinion
Velocity, in./min	2.0
Total movement, in.	14.0
Scram drive	Gravity
Long-term reactivity effects (from clean to 2% burnup)	
Burnup of U-235 in core, $\Delta k/k$	-0.02
Buildup of plutonium in core, $\Delta k/k$	+0.002
Buildup of plutonium in blanket, $\Delta k/k$	+0.0072
Buildup of fission products, $\Delta k/k$	-0.002
Irradiation growth of fuel (4% growth), $\Delta k/k$	-0.011
Heat Transfer	
Heat generation in reactor	53.5
Core, control, and safety subassemblies, MW	53.5
Upper and lower blanket, MW	1.5
Inner blanket, MW	6.1
Outer blanket, MW	1.4
Neutron shield, MW	0.03
Heat generation in core	
Radial maximum-to-average power density at reactor center plane	1.46
Axial maximum-to-average power density at reactor centerline	1.15
Power density, average, MW/liter	0.735
Power density, maximum, MW/liter	1.23
Power density, maximum to average	1.67
Specific power, MW/kg	0.311
Fuel elements, surface area, ft^2	260
Control elements, surface area (in active zone), ft^2	32.4
Safety elements, surface area, ft^2	6.6
Total surface area, ft^2	299
Maximum heat flux, Btu/(hr)(ft^2)	929,000
Average heat flux, Btu/(hr)(ft^2)	619,000

REFERENCES

1. L. J. Koch, H. O. Monson, D. Okrent, M. Levenson, W. R. Simmons, J. R. Humphreys, J. Haugsnes, V. C. Jankus, and W. B. Loewenstein, *Hazard Summary Report Experimental Breeder Reactor II (EBR-II)*, ANL-5719 (May 1957).

2. L. J. Koch, W. B. Loewenstein, and H. O. Monson, *Addendum to Hazard Summary Report, Experimental Breeder Reactor II (EBR-II)*, ANL-5719 (Addendum) (June 1962).

3. R. A. Blaine and R. F. Berland, *Simulation of Reactor Dynamics Volume 1. A Description of AIROS-IIA*, NAA-SR-12452 (Sept. 5, 1967).

4. *EBR-II System Design Descriptions*, Argonne National Laboratory (Internal Communication).

5. P. J. Persiani, "Nuclear Analysis Methods Development," in *Reactor Development Program Progress Report*, pp. 43-48, ANL-7419 (Jan 1968).

6. D. F. Schoeberle, J. Heestand, and L. B. Miller, *A Method of Calculating Transient Temperatures in a Multiregion, Axisymmetric, Cylindrical Configuration, the ARGUS Program, 1089/RE 248, Written in FORTRAN II*, ANL-6654 (Nov 1963).

7. J. A. DeShong, Jr., *Dynamic Analysis of Liquid-metal-cooled Fast Power Reactors*, ANL-7529 (Jan 1969).

8. G. H. Golden and J. V. Tokar, *Thermophysical Properties of Sodium*, ANL-7323 (Aug 1967), p. 43.

9. S. T. Zegler and M. V. Nevitt, *Structures and Properties of Uranium-Fissium Alloys*, ANL-6116 (July 1961).

10. H. Savage and R. D. Seibel, *Heat Capacity Studies of Uranium and Uranium-Fissium Alloys*, ANL-6702 (Sept 1963).

11. F. J. Hetzler *et al.*, *Thermal Conductivity of Uranium and Uranium-Plutonium Oxides*, GEAP-4879 (Aug 1967).

12. F. J. Tebo, *Selected Values of the Physical Properties of Various Materials*, ANL-5914 (Sept 1958).